Spring 2015

Effect of polymer on disproportionate permeability reduction to gas and water for fractured shales

Lingbo Liu

Department:

EFFECT OF POLYMER ON DISPROPORTIONATE PERMEABILITY REDUCTION TO GAS AND WATER FOR FRACTURED SHALES

by

LINGBO LIU

A THESIS

Presented to the Faculty of the Graduate School of the

MISSOURI UNIVERSITY OF SCIENCE AND TECHNOLOGY

In Partial Fulfillment of the Requirements for the Degree

MASTER OF SCIENCE IN PETROLEUM ENGINEERING

2015

Approved by

Dr. Baojun Bai, Advisor

Dr. Mingzhen Wei

Dr. Zhaojie Song

ABSTRACT

Large volumes of fracturing fluid are required in shale slickwater fracs, and a considerable amount of polymer friction reducer would remain in microfractures if the polymer has not been broken before gas production. It is of major interest to evaluate the effect of polymer on water/gas flow behavior in the microfractures of shale reservoirs. We fabricated six shale fracture models with different fracture widths and set up a core flooding apparatus to conduct brine/gas-injection experiments before and after polymer treatment. A method by which to calculate the residual resistance factor for gas ($F_{rr,gas}$) was defined. The experimental results illustrate that polymer can reduce the permeability to water more than to gas. In the first cycle of brine/gas injection experiments after polymer treatment, the residual resistance factor for brine ($F_{rr,water}$) and $F_{rr,gas}$ exhibited power-law characteristics through their shear rate and superficial gas velocity, respectively. The $F_{rr,water}$ and $F_{rr,gas}$ tended to decrease as the fracture width grew. Surprisingly, the $F_{rr,gas}$ was less than one in larger fractures in which $F_{rr,gas}$ tended to stabilize after polymer treatment, which indicates that polymer treatment does not impair gas flow in wider fractures, and may even improve it. The mechanisms responsible for disproportionate permeability reduction (DPR) in the fractured shales were proposed in this paper.

ACKNOWLEDGEMENTS

This thesis would not have been possible without the help and constant support of my advisor Dr. Baojun Bai. I thank him for accepting me as one of his graduate students and constantly guiding me with utmost patience to become a better Engineer.

I am also thankful to my comittee members Dr Mingzhen Wei and Dr. Zhaojie Song for providing their timely guidance.

And last but not the least, I would like to sincerely acknowledge my parents. Without their blessings pursuing an Engineering degree would not have been possible.

TABLE OF CONTENTS

LIST OF ILLUSTRATIONS

LIST OF TABLES

NOMENCLATURE

Symbol	Description
A	Cross-sectional area
cP	Centi-poise
dP/dL	Pressure Gradient
EIA	US Energy Information Administration
Frr	Residual resistance factor
gpt	Gallon per thousand gallon
h	Fracture height, m
K	Absolute Permeability
Kw	Relative permeability
q	Fluid flow rate
tcf	Trillion cubic feet
v	Fluid velocity
γ	Shear rate, s-1
ΔP	Pressure drop
ρ	Fluid density
mD	Milli-Darcy
DPR	Disproportionate Permeability Reduction
PR	Polymer residence time
WPR	Without polymer residence time
HPAM	Polyacrylamide
D	Diameter
L	Length of the shale fracture model
U	Superificial velocity
Q_{gsc}	Gas flow rate
P_{base}	Base pressure (Atmospheric pressure)
$F_{rr,water}$	Residual Resistance Factor for brine
Q	Water flow rate
Q_g	Gas flow rate
P_{in}	Inlet pressure
P_{out}	Outlet pressure (Atmospheric pressure)

ΔP_a	Brine-injection pressure drop after the polymer treatment
ΔP_b	Brine-injection pressure drop before the polymer treatment
W_f	Fracture width
μ_g	Gas viscosity at the condition of P_{base}
nD	Nano-Darcy
KCL	Potassium Chloride

1. INTRODUCTION

Shale gas refers to natural gas that is trapped within shale formations. Shales are fine-grained sedimentary rocks that can be rich sources of petroleum and natural gas. Over the past decade, the combination of horizontal drilling and hydraulic fracturing has allowed access to large volumes of shale gas that were previously uneconomical to produce. The production of natural gas from shale formations has recovered the natural gas industry in the United States.

We proposed this research because of the effect of polymers on the permeability of water and hydrocarbon. It is well documented that polymers in the form of either solutions or gels have the function to reduce the permeability to water more than that to oil and gas, which is referred to as disproportionate permeability reduction (DPR) (Bai B et al 2007). Several experimental studies were conducted to confirm adsorption-entanglement and blocking are the basic mechanisms by which polymer layer on pore/fracture walls can modify flow characteristics and thus preferentially reduce the water relative permeability (Zaitoun A et al 1988). Hence, polymer treatment has been proven to be a cost-effective technology for reducing water production in conventional oil and gas reservoirs. It is expected that this technology will also have great potential for controlling water production in shale gas reservoirs. However, shale gas reservoirs are quite different from conventional sandstone and carbonate reservoirs in that their flow paths are fractures or micro fractures rather than networked pore spaces and throats. Therefore, the results of current DPR research in conventional cores may not apply to shale gas without further laboratory research and testing. Recently, the idea of combining DPR with hydraulic fracturing or acid treatments to reduce water production after stimulation treatments has generated much interest. It could be promising to combine polymer treatment and

hydraulic fracturing into one process for shale reservoirs that have or could have water production problems, especially for those that require re-fracturing. The objective of the study presented in this thesis was to test whether a polymer can reduce gas permeability and the extent to which a polymer can reduce permeability to water more than to gas in fractured shales. It is expected that this research will extend the knowledge of polymer DPR from conventional, un-fractured rocks to the fractured system.

2. LITERATURE REVIEW

2.1. THE IMPORTANCE OF SHALE GAS

The great success of shale gas in the U.S has changed the global energy situation. Accepted estimates show that shale gas production will increase from 9.7 Tcf (trillion cubic feet) in 2012 to 19.8 Tcf in 2040 (EIA 2014), acting as the largest contributor to the increase in the total natural gas production in the U.S. Correspondingly, the percentage of shale gas making up the total natural gas production in the U.S. will grow from 40% in 2012 to 53% in 2040 (See Figure 2.1). Because a shale matrix has low porosity and ultra-low permeability of 10^{-8}-10^{-4} mD, producing shale gas economically depends primarily upon hydraulic stimulation (Bai, B et al 2012) Hydraulic stimulation can generate fractures that connect with inborn fissures to create a fracture network, thereby exposing more of the shale matrix to stimulate gas production.

Shale gas will continue to be a vital energy source not only in the US but also the globe. With the shortage of the crude oil in recently years, the shale gas is becoming more important for different companies looking to manage their operating costs. However, there are still some complex problems and challenges currently being faced in the industry and the academic institutions to better understand the flow behavior and petrophysical properties of shale gas. Due to the prospect of shale gas development, the investment in researching and understanding the petrophysical properties of shale gas will bring us closer to access the world wide reserves. For the future field development, production forecasts and reserve estimations make it essential to understand the petrophysical properties of shale gas. In addition, the US will still lead the shale gas development. But eventually the recovery of shale gas will

play a great role in Asia and the rest of the world, where potential reserves are still not fully developed (EIA 2013).

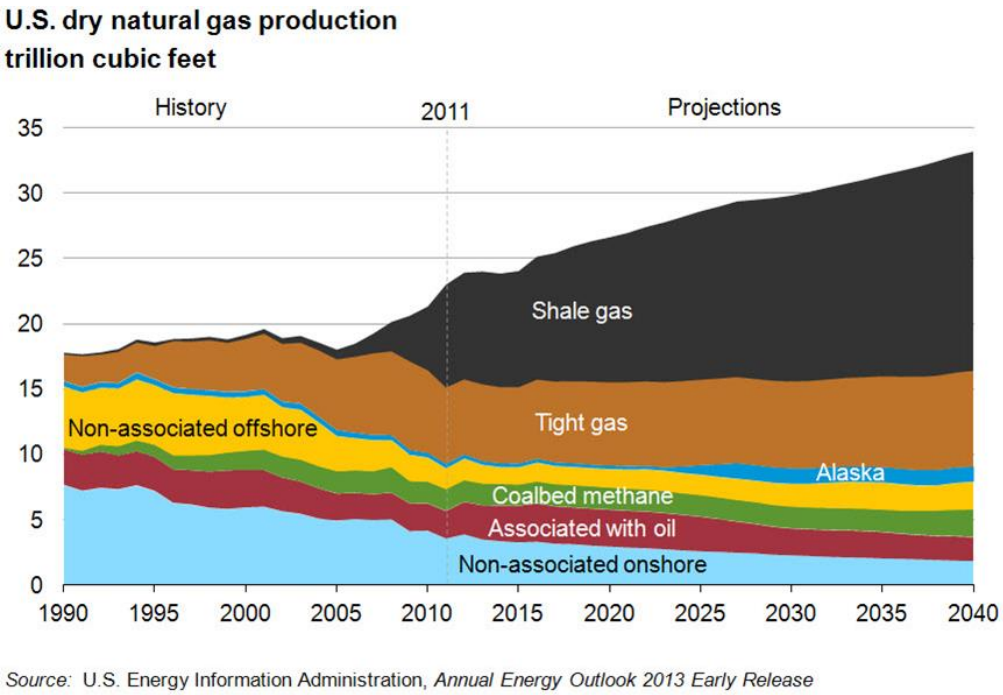

Figure 2.1. US Dry Natural Gas Production Prediction

2.2. WATER PROBLEM IN SHALE GAS RESERVOIRS

Excess water production in shale gas is one of the most prevalent operational problems that gas companies are facing (Bai 2011). Water production is generally due to the effect of natural heterogeneities, fractures or viscous fingering and it creates many problems, such as water blocking, phase trapping, and liquid dropout in the wellbore. These problems could build back pressure on the formation causing the wells to be shut off. Polymers and polymer gels have been used widely to control excess water production in conventional hydrocarbon production assets. Water/oil or water/gas flows in porous media are strongly modified in the presence of polymers or polymer gels in the pore.

2.3. HYDRAULIC FRACTURING AND WATER CONTROL

Hydraulic fracturing technology is used to fracture the shale and create pathways that enable the trapped gas to migrate to the well. The fractures are created by pumping large volumes (up to several millions of gallons) of fluid at high pressure down the wellbore and into the gas-bearing shale. These fluids are commonly water-based that contains chemicals to control the fluid's physical properties and possible reactions with the shale. In addition to chemicals, the fluid carries small solid particles such as sand grains known as "proppants". These props sustain the fractures and enable gas to flow through them after formation closed and the pressure decreased.

With the advantage of reducing both costs and formation damage, slickwater fracturing is an effective stimulation method applied most widely to improve production performance and economics in shale gas reservoirs. In 1997, Devon Energy successfully introduced large-volume slickwater treatments into the Barnett shale, rather than cross-linked fracture treatments. Due to the lack of gel solids in the fracturing fluid, longer and more complex fractures formed, and no gel residue or filter cake was left to damage the fracture conductivity. However, slickwater fracturing provides poor proppant transport and limited stimulated reservoir volume due to the low viscosity of the fracturing fluid. To compensate for this disadvantage, high pump rates that may exceed 100 bbl/min are usually required to carry proppant in the fracturing fluid. A considerable amount of energy loss occurs due to the turbulence of the fracturing fluid, and additional pumping pressure is required to achieve the desired treatment. Therefore, friction reducers serve as one of the primary additives in slickwater fracturing fluid to reduce the fluid friction associated with high pump rates.

The slickwater fracturing fluid contains some specially designed additives. Their name, generic product, typical concentration, and function are shown in Table

2.1 (Arthur, Bohm et al. 2009, Paktinat, O'Neil et al. 2011, Paktinat, O'Neil et al. 2011).

Table 2.1. Composition of Fracturing Fluids

Additives	Generic chemistry	Typical concentration	Function and purpose
Water	Mixing fluid	~95-99%	Majority of frac fluids
Brine	KCl	0.2%	Create a brine carrier fluid that prohibits fluid interaction with formation
Friction reducer	Polyacrylamide (anionic, cationic or nonionic), Mineral oil	0.25-1 gpt	Reduce the flowing friction by changing the turbulent flow to laminar flow
Surfactant	Ethoxylated alcohols, Isopropanol	0.02-0.1%	Reduce the frac fluid surface tension, and improve the liquid recovery from the well after frac
Breaker	Peroxide, Enzyme complexes	0.009%	Allow a delayed break down of the polymer and gel
Biocide	Glutaraldehyde, DBNPA, THPS, Dazomet.	0.01%	Eliminates bacteria in the water that produce corrosive byproducts
Crosslinker	Borate salts	0.006%	Maintain the fluid viscosity as temperature increase

The most common friction reducers are polyacrylamide based and usually are anionic, cationic or nonionic. A friction reducer can modify the mean velocity profile in pipelines and redistribute the shear in the boundary layer. As a result, the near-wall structure of the turbulent boundary layer changes significantly to minimize energy loss via the polymer friction reducer interacting with eddies of turbulent flow. The friction reducer is loaded into the slickwater fracturing fluid at a concentration of 0.25

to 2gpt (gallon per thousand gallons), thereby reducing the friction in the wellbore by as much as 80% compared with fresh water.

There are three major factors to evaluate a friction reducer: friction reduction, leak-off control and apparent viscosity. Five types of friction reducer are compared in Table 2.2.

Table 2.2. Comparison of Five Types of Friction Reducer (White 1964)

	Base fluids	Friction reduction	Leak-off control	Apparent viscosity	Concentration
Guar	Aqueous	Not the most efficient	Good	Good	5 to 50 lb/ 1,000 gal
Anionic synthetic polymers	Aqueous	Most efficient in fresh water	Not good	More shear sensitive	2 to 4 lb/1,000 gal
Nonionic synthetic polymers	Aqueous	Between Anionic and Guar	Poor	Poor	2 to 4 lb/1,000 gal
Synthetic polymer solutions	Hydrocarbon	Efficient	No	No	3 to 8 lb/1,000 gal
In situ soap gels	Hydrocarbon	Not the most efficient	Good	Good	

The current practice is to use breakers to break the polymer during flowback because it is commonly believed that the polymer has a negative effect on gas productivity. Actually, a large volume of friction reducer could still remain in the micro-fractures in shale reservoirs after flowing back if the breakers cannot completely break down the polymers. Breakers degrade polymers by cleaving the polymeric macromolecule into small fragments which can be produced after the hydraulic fracturing during fluid recovery.

However, no research has been conducted to determine whether polymer can reduce gas permeability in fractured shales if the polymer has not been broken before gas production. Therefore, it is of major interest to find a way to evaluate the effect of polymer on water/gas flow behavior in the micro-fractures of shale reservoirs which hold the majority of the productivity potential of shale gas.

2.4. MECHANISM OF DISPROPORTIONAT PERMEABILITY REDUCTION

Table 2.3. Mechanism Summary for Disproportionate Permeability Reduction (Bai, et al 2014)

NO	Mechanism	Gel	Investigator
1	Gel swells in water but shink in oil	Cr(III)-acetate HPAM; Xanthan gum	Liang et al; Dawe and Zhang; Gales et al; Sparlin and Hagen
2	wall effect	polyacrylamide polymers; water and oil based gel	Zaitoun et al; Liang and Seright
3	gravity effect	cationic polyacrylamide (CPAM)	Liang et al
4	wettability effect	Nonionic polyacrylamide (PAM) resorcinol form	Zaitoun et al; Liang et al
5	Effect of capillary forces and gel elasticity	Cr(III)-acetate HPAM; Bulk polymer gel	Liang and Seright
6	Lubrication effect	PAM and polyacrylamide polymer	Zaitoun and Kohler; Sparlin and Hagen
7	Gel dehydration	PPG, acetate/HPAM	Dawe and Zhang;
8	Segregated flowpathway	polymer, water and oil based gel HPAM	white,J.L et al. Liang and Seright. Nilsson et al.
9	gel droplets	water and oil based gels.	Liang and Seright

Many mechanisms for polymer and polymer gel DPR have been proposed and summarized in Table 2.3 (Bai, et al 2014).

2.4.1 Gel Swelling in Water but Shrinking in Oil. Sparlin and Hagen (1984) proposed that water-based gels swell in water and shrink in oil. The most obvious method to test for shrinking/swelling effects is to observe volume changes in a gel when it comes into contact with water or oil. If gels swell in water and shrink in oil, the increased system pressure might inhibit the gel from swelling in the presence of water. Thus, as the system pressure is raised, F_{rrw} should decrease. To investigate this concept, Liang, R.S Seright (1995) performed oil/water flow experiments in a high permeability Berea core at different backpressures.

Table 2.4. Effect of System Pressure on Frr (Liang, R.S Seright 1995)

Backpressure (psi)	Frro	Frrw
0	9	18×U E(-0.18)
500	9	16×U E(-0.26)
1000	11	18×U E(-0.31)
1500	11	15×U E(-0.24)
Gelant; 1.39% HPAM/0.212% Cr (III) as acetate		
All test run at 105°F U; Superificial velocity		

Table 2.4 shows that the *Frro* values were Newtonian and insensitive to system pressure. The lower *Frro* values were caused by the gel breakdown, while the F_{rrw} values exhibited strong apparent shear thinning behavior which can be described with a power law equation. F_{rrw} values also were insensitive to system pressure, which suggest that gel shrinking/ swelling might not be the valid mechanism.

However, Bai et al 2014 observed a different trend for PPG (performed particle gel), in visualization studies with PPG at atmospheric pressure, significant

volume changes in the gel has been observed. In brine, dry gel swelled to many times its original size, which helps to increase the residual resistance factor for water. After that, if put swollen particle gel in a glass container filled with oil for three weeks, the gel volume decreased dramatically to half of its original PPG volume. The shrinkage of the gel particle size volume allows oil to move easily through gel and causes more permeability reduction to water than oil. In this study, gel strength plays an important role for PPG that greatly affects the DPR. Results obtained from rheometer measurements suggest that the gel strength for oil was much higher than for water, gel with less strength has a lower residual resistance factor than gel with high strength.

2.4.2 Segregated Flow Path to Water and Oil in Porous Media. It is said the water-based gel will follow the water preferred pathways and block these more than the oil channels; following the same logic, an oil-based gel reduces the permeability for oil more than for water. The factors that govern which channels that are oil or water preferred are the wettability and pore size. Since water-based polymers will be trapped in part of pore space available for water, the water flow restriction is stronger than the restriction for oil. After treatment, oil will continue to flow in the large pores with minimum restriction. But the water flow is restricted both in the small pores and pore channels due to water based gel effect which will result in a DPR (Liang and Seright, 1997, Liang 1995, White 1973 ; Schneider and Owens 1982; Nilsson 1998; Stavland and Nilsson, 2001).

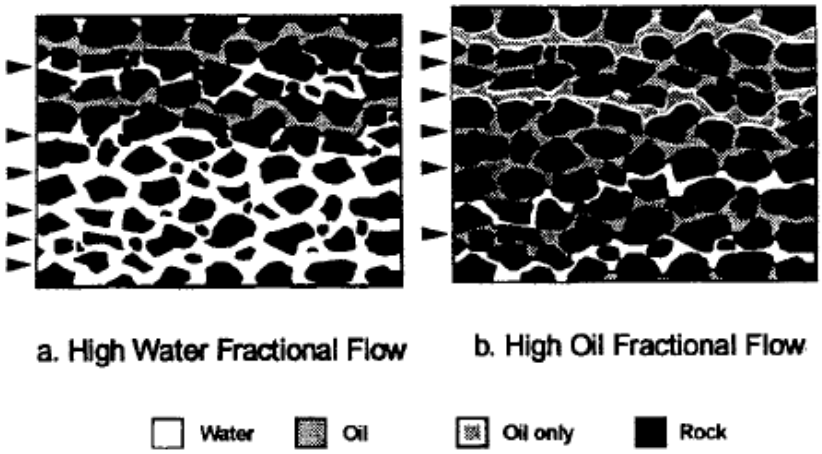

Figure 2.1. Segregate Water and Oil Pathway (Liang and Seright, 1997)

If this segregated pathway theory is valid, the disproportionate permeability reduction could be enhanced by simultaneously injecting oil with a water based gelant or water with an oil based gelant. Assume simultaneous injection of water and an oil based gelant should allow a large fraction of water pathways to remain opened than injection of oil based gelant itself or simultaneous injection of oil and water based gelant will enhance DPR effect than injecting water based gelant only.

To test this theory, two different experiments were performed using high permeability Berea sandstone cores by Liang and Seright (1997). The first experiment used oil based gel that contained 18% 12-hydroxystearic acid in Soltrol 130. Results are show in Table 2.5

Table 2.5. Frrw and Frro Values for Oil Based Gel in Berea Sandstone (Liang and Seright 1997)

Gelant/water Volume ratio	Kw (md)	First Frrw	First Frro	Second Frrw	First Frro/Frrw
100/0	599	34	300	30	9
50/50	586	5	225	14	45
Gelant; 18% 12-Hydroxystearic acid and Soltrol 130					

Table 2.5 shows that for the case where brine was injected with gelant (using a 50/50 volume ratio), the water residual resistance factor (Frrw=5) was much lower than the case where no brine was injected with the gelant (Frrw=34). These results indicate that the DPR was enhanced by the simultaneous injection of water with an oil based gelant which support the segregated pathway theroy.

The similar experiments has been performed using a water based gel to test this theory. If the theory is valid, simultaneous injection of oil and water based gelant should enhance the DPR. Four core experiments were conducted in high permeability Berea sandstone cores using Cr(III)-acetate-HPAM gel. Results are shown in Table 2.6.

Table 2.6. Frrw and Frro Values for Water Based Gel in Berea Sandstone (Liang and Seright 1997)

Gelant/oil volume ratio	Kw (md)	First Frro	First Frrw	Second Frro	First Frrw/Frro
100/0	793	42	2450	37	58
95/5	655	390	11100	500	28
50/5	520	27	1255	16	46
37/70	622	26	1075	20	41
Gelant;0.5% GPAM, 0.0417% Cr(III) acetate, 1% NACL					

For the data collected in 95/5 gelant oil ratio, an error may exist in measuring Frro and Frro. However, from the trend that simultaneous injection of oil with a water based gelant using gelant/oil injection ratios of 100/0, 95/5, 50/50, and 30/70 failed to enhance the DPR and this findings do not support the segregated pathway theory due to all the experiments are conducted using strongly water wet cores. And it will more

convincing for using mixed wet cores. Nevertheless, with any wettability, the segregated pathway theory predicts that oil and water phases take different flow paths on a microscopic scale still need futhur investigation.

Similar experiments were done by S. Nillsson et al (2003) and their results supported the mechanism of segregated pathways for oil and water.

Table 2.7. Experiment Arrangement for Segregated Pathway Theory (S. Nillsson et al 2003)

Water	synthetic sea water with a total salinity of 43,4g/litre of 24.8g/litre NACL
oil	white oil
gelants	A) polyacrylamide (HPAM) with add crosslinker
	B) Biopolymer
sandpack	D-2cm, L-30cm 1) quartz sand (water wet), 2) Teflon power only (oil wet) 3) mixture of quartz & Teflon 4) sandwich
cores	original k 2000mD, Ø, 45-55% T, 23°C

Table 2.8. Effect of Gel Treatment on Different Wet Systems (S. Nillsson et al 2003)

Experiment	RRF	Endpoint permeability (md) for oil befor and after gel	Endpoint permeability (md) for brine befor and after gel	Sw at gel placement
1. oil-wetting, gel placed at 25% Sw	RRFw =810	KO=301 (Sw=0.12)	Kw=1622 (Sw-0.5)	
	RRFo =50	KO'=5.7 (Sw=0.15)	Kw'=2 (Sw=0.48)	0.25
2. oil-wetting, gel placed at 40% Sw	blocking	KO =70 (Sw=0.17)	Kw=371 (Sw=0.7)	0.4
3. Fractional wetting, gel placed at Sor	RRFw =1000	KO =2136 (Sw=0.21)	Kw=2618 (Sw=0.6)	
	RRFo =16	KO' =132 (Sw=0.43)	Kw'=2.7 (Sw=0.63)	0.6
4a. Fractional wetting, gel placed at high So by co-injection	RRFw =50	KO =1172 (Sw=0.07)	Kw=1309 (Sw=0.55)	
	RRFo =4	KO' =307 (Sw=0.21)	Kw'=28 (Sw=0.55)	0.36
4b. Fractional wetting, gel placed at high So by co-injection	RRFw =3	KO =1404(Sw=0.05)	Kw=1698 (Sw=0.49)	
	RRFo =1.1	KO' =1234(sw=0.15)	Kw'=559 (Sw=0.47)	0.52
5a. Fractional wetting, gel placed using surfacrtant to reduce endpoint So	RRFw =12900	KO =1941(Sw=0.08)	Kw=2527 (Sw=0.49)	
	RRFo =9240	KO' =0.21 (sw-0.02)	Kw'=0.2 (Sw=0.55)	0.55
6. water wetting, gel placed at Sor	blocking	KO =2200 (Sw=0.24)	Kw=1875 (Sw=0.78)	0.78
7. sandwich, gel placed at Sor	RRFw =232	KO =2892 (Sw=0.15)	Kw=4224 (Sw=0.57)	
	RRFo =10	KO' =292 (Sw=0.36)	Kw'=17.7 (Sw=0.51)	0.53

From the Table 2.8, the first two experiments were conducted in same condition but the gelant was placed at higher water saturation in the second round. The first experiment results showed significant DPR effect, and the second experiment results indicated that the core was completely blocked after gel treatment. It was not possible to obtain any flow through the core and therefore impossible to evaluate any DPR effect because high water saturation. For the fractional wetting system, the results were quite favorable, although the results showed different value for different fractional flow (experiment 3, 4 in Table 2.8). It clearly demonstrated that quite useful results could be obtained by placing the gelant with a coinjection of oil and gelant. For the experiment 5a, the gelant was placed at higher water saturation by the injection of surfactant, after the surfactant flooding, brine was injected again to wash out the surfactant, thus minimizing the possibility of any side effect from the surfactant, and the gelant was injected after the surfactant had been washed out. Results showed that the gel dramatically reduced permeability for both oil and water. The large permeability reduction can be attributed to the surfactant which washed away extra oil allowing the gelant to block most of the remaining oil channels. For the water wetting system in experiment 6, the result was also complete blocking after gel treatment due to high water saturation. The sandwich type of packing as mixed wettability also has favorable DPR effect.

It has been concluded that DPR effects can be understood in terms of segregated flow of water and oil. The factor that govern which channels that are oil or water preferred are the wettability and pore sizes. In a relative ranking, the best DPR effect is obtained in fractional wetting cores followed by oil wetting. Because it is very important to preserve oil continuous channels after a gel treatment, this is easiest to achieve in fractional or mixed wetting cores since the difference between oil and

water preferred pathways is enhanced compared to homogeneous wetting, where pore size is the only factor. In a homogeneous wetting phase, it is obviously easier to maintain oil continuous channels in an oil wet core than in a water wet core, because in a water wet core all narrow channels and especially narrow pore throats will be blocked by water-based gel, resulting in a blocking towards both oil and water.

2.4.3 Wall Effect Model and Gel Droplet Model. Zaitoun et al (1998) attributed the disproportionate permeability reduction to wall effects resulting from an adsorbed polymer layer on the pore walls. Figure 2.3 show that in a strongly water wet rock; residual oil droplets at the center of the pores can reduce the effective width of the water channel during water flooding. But it will not restrict oil flooding because oil droplet will reconnected. Thus the wall effect model could explain why some water-based gels exhibit disproportionate permeability reduction in strongly water wet cores. Following the same logic, Figure 2.4 illustrated that the wall-effect model for oil-based gel reduced the permeability to oil more than water in a strongly oil-wet core. These findings suggest that the wall-effect model can explain the DPR when the gel is prepared for the wetting phase.

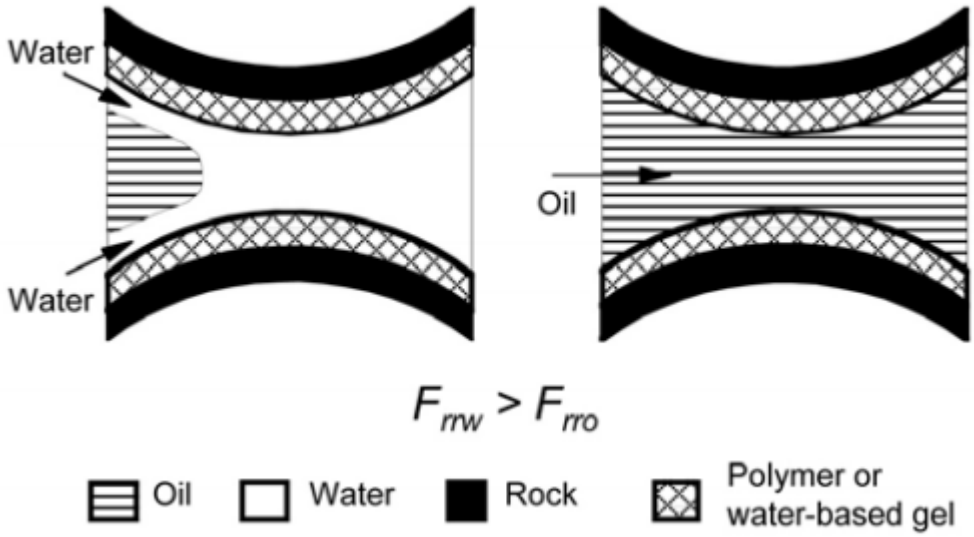

Figure 2.3. Wall-Effect Model; Water Based Gel with Water-Wet Rock (Zaitoun et al 1998)

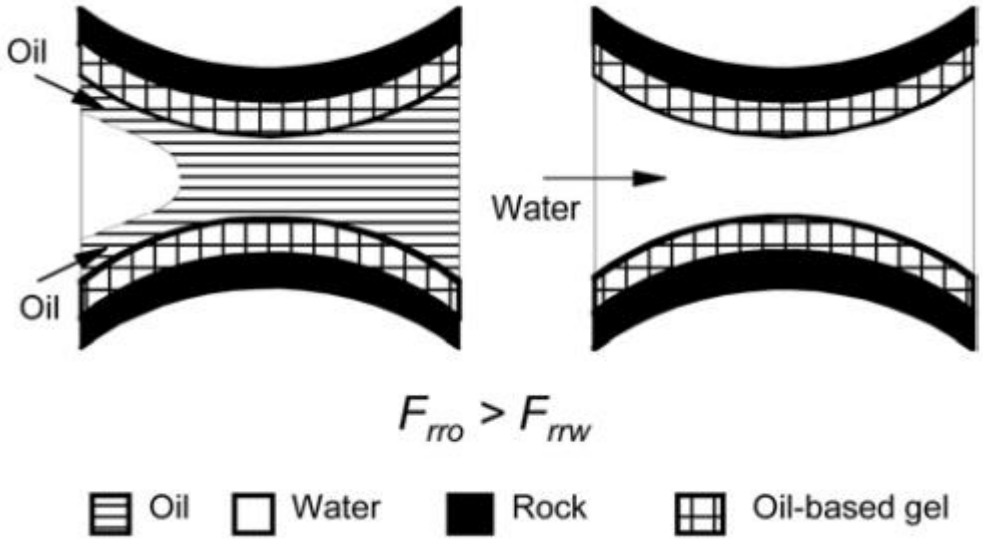

Figure 2.4. Wall-Effect Model; Oil Based Gel with Oil Wet Rock (Zaitoun et al 1998)

In order to study the effect of polymer adsorption on reducing water permeability, a series of experiments were performed by A.L.Ogunberu et al (2004) in sand packs and Berea sandstone for comparison purpose. The experiments were

aimed at determining permeability reduction to brine under static adsorption and dynamic adsorption.

Table 2.9. Material for Polymer Adsorption Experiment (A.L.Ogunberu et al 2004)

Material	
brine solutions	1% Nacl brine
polymer solutions	Alcoflood 935 polymer 5000ppm
porous medium	ASTM graded sand pack
	Berea sandstone core

Table 2.10. Residual Resistance Factor (RRF) Summary for 5000 ppm Alcoflood 935 Polymer in Sand-pack with and without Polymer Residence Time, Brine Injection at 0.8ml/min (A.L.Ogunberu et al 2004)

Polymer effective shear rate, S^{-1}		RRF (PR-30min)	RRF (WPR)
PR	WPR		
65	66	2.22	1.02
135	135	2.64	1.1
277	295	2.93	1.57
660	596	5.86	1.63
1418	1213	7.81	1.74
*PR; with 30 min polymer residence time *WPR; without polymer residence time			

Table 2.10 presents RRF summary for 0.8 mL/min brine flow with and without polymer residence time. The permeability reduction and RRF values with increasing shear rate show corresponding trend with the adsorbed layer thickness. The RRF values were fairly constant at low shear rates and then increased with increasing shear rate. It is observed that the RRF values at low shear rates when polymer

residence time is allowed is twice that without polymer residence time and increases 4 times at high shear rates which suggest DPR effect are enhanced by polymer adsorption time.

Table 2.11. Residual Resistance Factor (RRF) Summary for 5000ppm Alcoflood 935 Polymer in Sand-Pack with and without Polymer Residence Time, Brine Injection at 2.0mL/min

Polymer effective shear rate, S^{-1}		RRF (PR-30min)	RRF (WPR)
PR	WPR		
53	65	1.62	1.37
228	264	2.11	1.44
468	546	2.35	1.65
1037	1185	3.52	2.28
2107	2521	3.76	2.92
*PR; with 30 min polymer residence time *WPR; without polymer residence time			

The RRF summary for 2.0mL/min brine flow rate is presented in Table 2.11 DPR effect is observed in the RRF values between polymer residence time and without polymer residence time by a factor of about 1.5 from low to high shear rates. However, it is not significant compare to flow rate at 0.8ml/min which suggest high brine flow rate wash out the adsorbed polymer layer make fluid easily go through resulting low DPR.

The above trends and RRF values indicate that the increase in adsorbed polymer layer thickness will maximize permeability reductions when polymer residence time is allowed. For comparison with the above results, the effect of polymer concentration and the effect of shear rate were also studied.

Table 2.12. Residual Resistance Factor (RRF) Summary for 10000 ppm Alcoflood 935 Polymer in Sand-Pack with Polymer Residence Time, Brine Injection at 2.0mL/min

Polymer effective shear rate, S^{-1}	RRF (PR-30min)
58	2.26
117	2.4
242	2.72
479	2.6
928	2.29
1817	2.1

Table 2.13. Residual Resistance Factor (RRF) Summary for 500 ppm Alcoflood 935 Polymer in Berea Sandstone Core with Polymer Residence Time, Brine Injection at 0.5 mL/min

Polymer effective shear rate, S^{-1}	RRF (PR-30min)
150	5.85
302	6
601	5.92
1202	5.91
1503	5.92
2411	5.97

The RRF values are summarized in Table 2.12 which indicates increase in polymer concentration did not affect the residual resistance factor. For low polymer concentration in Berea sandstone (500ppm) results show in Table 2.13 suggests shear rates have less influence on residual resistance factor. However, it does affect the sand-pack residual resistance which indicates shear rate is not the only factor that influences DPR.

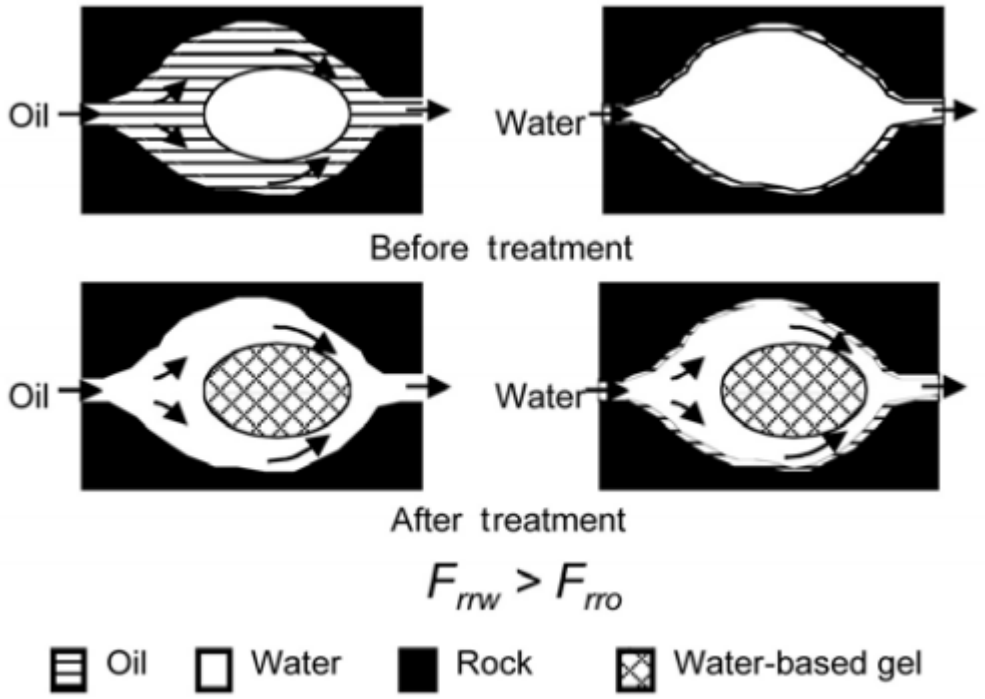

Figure 2.5. Gel-Droplet Model; Water-Based Gel with Oil-Wet Rock (Nilsson et al 1998)

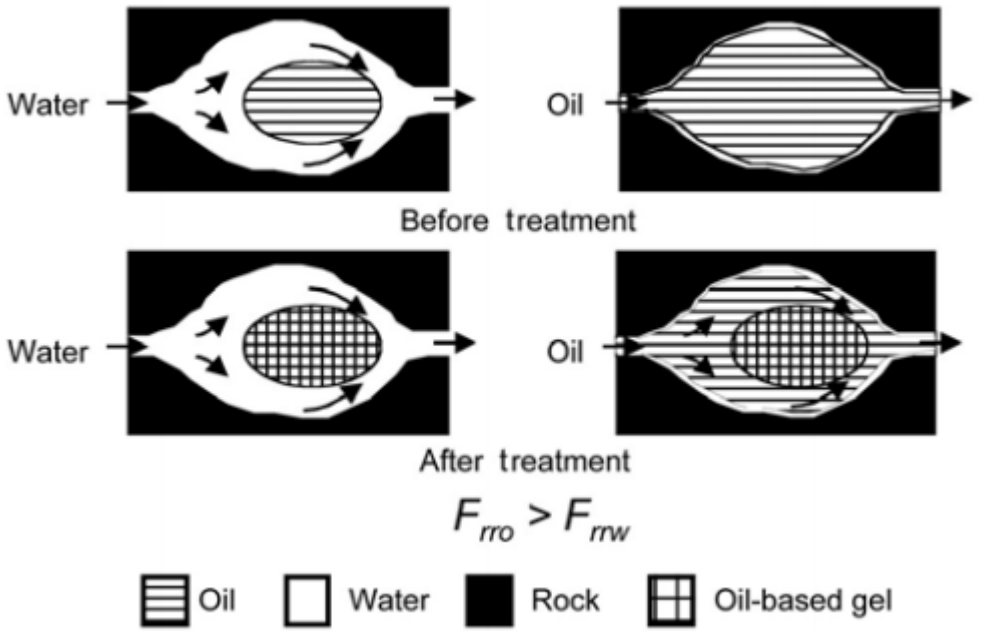

Figure 2.6. Gel-Droplet Model; Oil-Based Gel with Water-Wet Rock (Nilsson et al 1998)

For gel droplet model in Figure 2.5 and Figure 2.6, a gel droplet forms at the center of the pore, causing more restriction to flow of the wetting phase than to flow of the non-wetting phase, to clarify the difference between the wall-effect model and the gel-droplet model, polymer or gel adheres to the pore walls in the wall-effect model other than in the center of the pore (J. Liang and R.S. Seright 2000). Consider the case where a water-based gel is used to treat an oil-wet core, before gel treatment, when water flows through an oil-wet pore, the only restriction to water flow is a thin film of residual oil on the pore walls. However, when oil flows through the same pore, a residual water droplet in the pore restricts oil flow. After gel treatment, a gel droplet forms at the center of the pore. Replacing the residual water droplet (the gel is the non-wetting phase). If the size of the gel droplet is the same as that of the residual water droplet, the volume fraction of the pore available to oil flow remains the same as before treatment, However, it significantly reduce the water flow by the presence of gel droplet. Thus, the gel can reduce permeability to water without affecting permeability to oil (Figure 2.5). Following the similar logic, Figure 2.6 illustrates an oil-based gel reduce the permeability to oil more than water in a strongly water-wet rock. These findings suggest that the gel-droplet model can explain the DPR when the gel is prepared for the non-wetting phase.

In a word, the wall-effect model applies for water-based gels in water-wet cores or for oil based gels in oil-wet cores. The gel droplet model applies for water based gels in oil-wet cores or for oil-based gels in water-wet cores. (Liang and Seright 2001);

2.4.4 Gel Dehydration during Oil Breakthrough. As Figure 2.7 suggests that oil permeability develops as oil penetrates into the gel-filled pore space, dehydrating the gel by displacing brine from the gel structure and creating new flow channels around gel. The new pore space is part of the original porosity, and the permeability to oil is reduced from its value before gel placement. Subsequent brine injection displaces oil from these flow channels but traps some of the oil in the new pore space as a residual saturation. The trapping of residual oil in the new pore space causes the disproportionate reduction in brine permeability because the brine flows primarily in the pore channels created by dehydration of the gel. When gelant is placed in a matrix containing residual oil, dehydration of the gel reconnects some of the trapped oil, and the oil permeability increases which result in favorable DPR effect (D.W Green et al 2002).

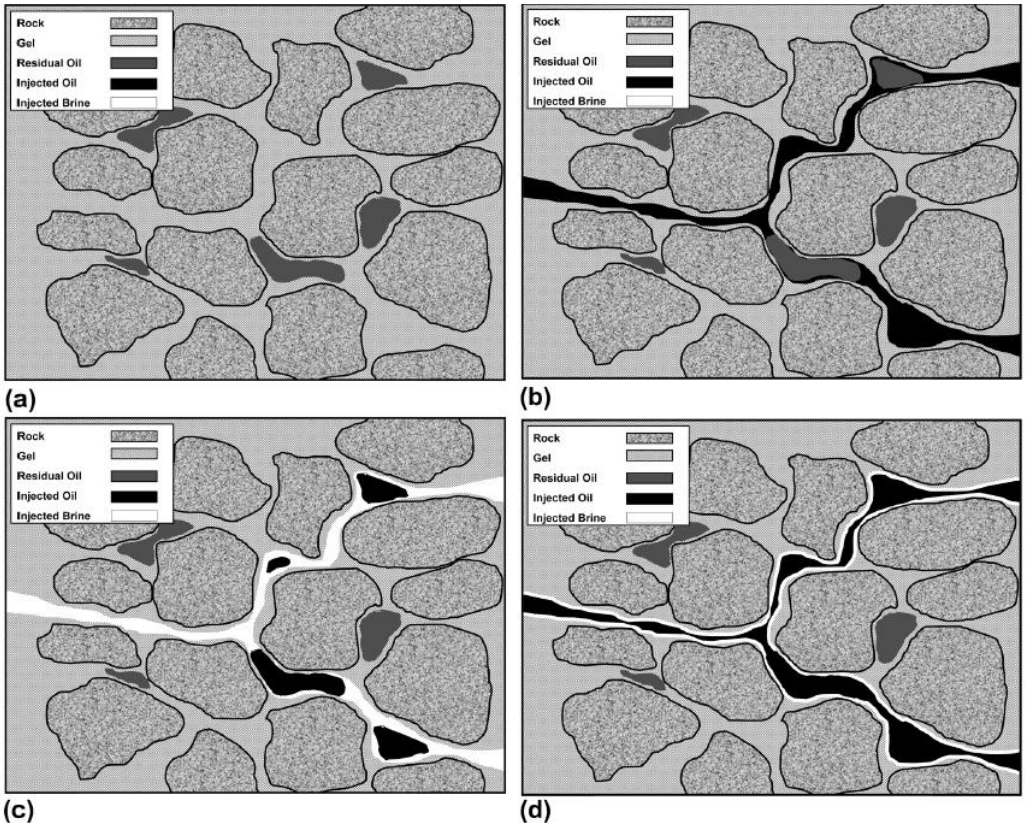

Figure 2.7. a) Encapsulation Of Water Flood Residual Oil Following In-Situ Gelation Of Chrome-Acetate-Polyacrylamide Gelant; B) Generation Of New Pore Space When Gel Is Dehydrated By Injection Of Oil; C) Trapping Of Residual Oil In New Pore Space During Brine Flood, Leading To Disproportionate Permeability Reduction Of Brine; D) Flow Paths Of Oil Through New Pore Space, Trapping Low Saturation Of Brine (Green, D. W.2002)

A series of experiments by Willhite,G.P et al, Green, D.W et al 2002 was designed to determine if the phenomena of gel dehydration is valid in the porous medium. Two sand-packs (SP19 and SP20) were prepared and treated with gelant. Dehydration of each sand-pack was done by injection of oil at a constant pressure.

Sand-pack (SP20) was conducted in a 6-in long sand-pack to compare dehydration of a gelled sand-pack that contained water flood residual oil saturation with a sand-pack without residual oil saturation (SP19), both experiments are conducted at 25°C for 3 days gelation and using 5000ppm Alcoflood935 gel solution with injection rate about 5ml/min.

Table 2.14. Dehydration of Chromium Acetate-Polyacrylamide Gel in Sand-Pack Sp19 (D.W Green et al 2002)

Run	Displacement	Vp (ml)	Vgel (ml)	O (%)	Sw (%)	So (%)	Ko (md)	Kw (md)
1	Brine injection before gel treatment	55		32	100	0		4670
2	Gel treatment	55	55		32			
3	Dehydration with oil @ 160 psi/ft	55	41	8	0	100	50	0

Table 2.15. Dehydration of Chromium Acetate-Polyacrylamide Gel in Sand-Pack-SP20 (D.W Green et al 2002)

Run	Displacement	Vp (ml)	Vgel (ml)	Ø (%)	Sw (%)	So (%)	Ko (md)	Kw(md)
1	Brine injection beore gel treatment	58		33	100			4324
2	oil flood	58		33	21	0		
3	water flood	58		33	62	79		1485
4	gel treatment	58	36	33		38		
5	Dehydration with oil @ 160 psi/ft	58	22	21	0	38	280	0
6	Brine flood @ 160 psi/ft	58	22	21	-	0	0	10

Results from SP19 and SP20 show that without initial oil saturation, the oil permeability after dehydration was 50md (SP19) compared with the 280md with initial oil saturation (SP20) at the same condition which indicate after gel treatment residual oil has been reconnected.

The Second set of experiments was conducted in high permeability Berea cores (500md) by Ganguly, S., Willhite, G. P. et al 2003 designed to determine permeability to oil and water at endpoint saturations before and after gel treatment. In

the first experiment (core B5), a residual hydrocarbon saturation was established prior to injection of gelant. In the second experiment (core B6), the core was saturated with brine prior to the gel treatment. Both experiments use Alcoflood935 polymer with concentration of 5000ppm HPAM.

Table 2.16. The Summary Results of Berea Core Test (core B5) (Ganguly, S., Willhite, G. P. et al 2003)

Experiment procedure	Volume of brine produced (mL)	Volume of oil Produced (mL)	Volume* of trapped oil produced (mL)	Volume of brine in core (mL)	Volume of gel in core (mL)	Volume of oil in core (mL)	Volume of trapped oil in core (mL)	S_w (%)	S_o (%)	S_{gel} (% of initial porosity)	S_{ot} (Encapsulated by gel) (% of initial porosity)	Volume of mobile fluid (mL)	Effective porosity (%)	k_w (md)	k_o (md)
Brine saturation				18.92	0	0	0.00	100	0	0		18.92	19.2	520	
Oil flooding	12.6			6.32	0	12.6	0.00	33	66.6	0		18.92	19.2		420.6
Brine flooding		6.7		13.02	0	5.9	5.90	69	31.2	0		13.02	19.2	57.85	
Buffer solution injection				13.02	0	5.9	5.90	69	31.2	0		13.02	19.2	57.85	
Gel placement					13.02	5.9	5.90	0	31.2	68.8	31.2	13.02	19.2	57.85	
Post gelation					13.02	5.9	5.9		31.2	68.8	31.2		0.		
Oil dehydration 1 at 20psi	1.1		1.18	0	11.92	7	4.72	0**	100**	63	24.95	2.28	2.3		4.62
Brine flood 1 at 20psi		1.7	0.04	1.7	11.92	5.3	4.68	24.3	75.7	63	24.71	2.32	2.4	0.0061	
Oil dehydration 2 at 20psi	1.93		0.64	0	11.69	7.23	4.04	~0	100	61.8	21.33	3.19	3.2		5.69
Brine flood 2 at 30psi		2.2	0.01	2.2	11.69	5.03	4.03	31.4	69.6	61.8	21.29	3.2	3.3	0.0064	
Oil dehydration 3 at 30psi	2.2		0.43	0	11.69	7.23	3.60	~0	100	61.8	19.02	3.63	3.7		13.08
Brine flood 3 at 40psi		1.3	0.01	1.3	11.69	5.93	3.59	18	82	61.8	18.99	3.64	3.7	0.0104	
Oil dehydration 4 at 40psi	2.2		0.26	0	10.79	8.13	3.33	~0	100	57	17.62	4.8	4.9		26.7
Brine flood 4 at 50psi		2.4	0.01	2.4	10.79	5.73	3.33	29.5	70.5	57	17.57	4.81	4.9	0.033	
Oil dehydration 5 at 50psi	2.4		0.20	0	10.79	8.13	3.13	~0	100	57	16.52	5	5.1		36.75

Table 2.17. The Summary Results of Berea Core Test (core B6) (Ganguly, S., Willhite, G. P. et al 2003)

experiment procedure	Sw (%)	Sgel (%)	So (%)	Ø (%)	Kw (md)	Ko (md)
brine saturation	100	0		18.1	494	
gel placement	0	100	100	18.1		
post gelation		100	28	0	0.02	
oil dehydration at20 psi	0			6.2		103
Brine flood at 20 psi	71			6.2	29.8	

Results from floods in Core B5 (Table 2.16) suggest with the presence of residual oil saturation which greatly reduces the water and oil. Certainly increase the pressure gradient cause increase in oil permeability and decrease in water permeability which will enhance the DPR effect. Results from floods in Core B6 (Table 2.17) show the effective porosity following dehydration by oil at 20 psi was 6.3%, and the permeability to oil was 103md. After the water flood at 20 psi, the residual oil saturation in the pore space created by dehydration of the gel was 28%, Permeability to water was 29.8md. These permeabilities are much higher than the permeabilities observed in core B5 under the same pressure gradient. The main reason is due to the residual oil saturation significantly block the flow path make it even harder for water to go through which greatly contribute to the DPR. However, the reason oil permeability in Core B5 is smaller than Core B6 at the same oil dehydration pressure (20psi) is still left unknown.

Previous work done by Willhite 2002; Seright et al. 2002, 2006 revealed that gels can dehydrate during oil injection, thus causing disproportionate permeability reduction. other experiment have been done by Seright, R. S 2006 to illustrate this effect.

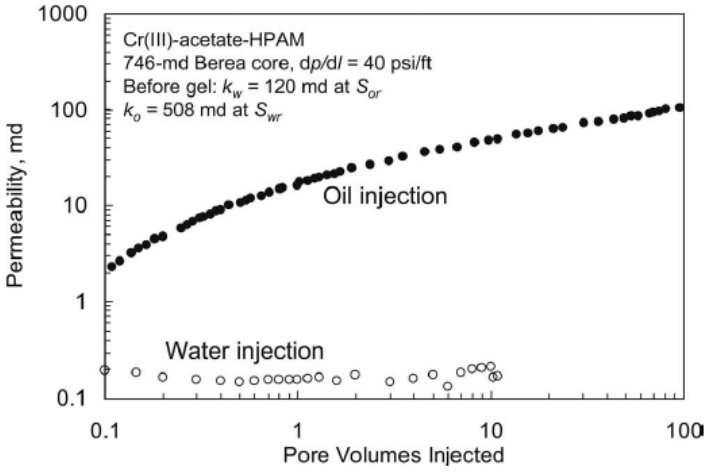

Figure 2.8. Permeability to Oil and Water after Gel Placement in Berea Sandstone (Seright, R. S 2006)

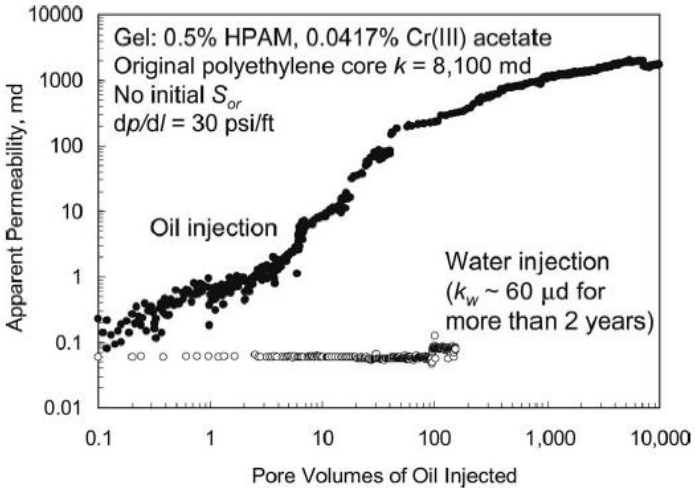

Figure 2.9. Permeabilities to Oil and Water after Gel Placement in Porous Polyethylene (Seright, R. S 2006)

Table 2.18. Summary of F_{rrw}/Frro after HPAM Gel Placement with Different Pressure Gradient (Seright et al 2006)

Entry	core material	Initial K(md)	Ø (%)	Kw at Sor Before gel	Ko at Swr Before gel	HPAM in gel (wt%)	dp/dl (psi/ft)	post gel Kw (md)	post gel Ko (md)	Frrw (md)	Frro (md)	Final Frrw/Frro
1	Berea	746	21	120	5080	0.5	40	0.17	105	706	4.8	147
2	Fused silica	1820	27	447	1240	0.5	30	0.23	307	1940	4	485
3	Fused silica	2390	27	640	1632	0.5	10	0.12	208	5330	7.8	683
4	Polyethylene	6400	40	4810	6400	0.5	100	0.32	515	15000	12.4	1210
5	Polyethylene	9530	40	5860	9530	0.5	30	0.24	531	24400	17.9	1363
6	Polyethylene	15270	40	6500	11410	0.5	10	0.37	637	17600	17.9	983
7	Berea	356	21	*	242*	0.5	13.7	0.015	209	23700	1.2	19800
8	Berea	389	21	*	389	0.5	30	0.005	330	77800	1.2	64800
9	Berea	100	21	*	68*	0.5	58	0.01	16.8	10000	4	2500
10	Berea	40	21	*	27.2*	0.4	58	0.019	13.4	2110	2	1050
11	Berea	274	21	*	186*	0.3	58	0.055	110	4980	1.7	2930
12	Berea	98	21	31	132	0.5	58	0.007	60.1	4430	2.2	2010
13	Berea	69	21	14.4		0.3	58	0.092		157		
14	Polyethylene	8100	40	*		0.5	30	0.06		135000		
15	Sand pack	8100	35	*	8100**	0.5	1.5	0.029	1840	279000	4.4	63400
16	Polyethylene	2000	40	*	2000**	0.5	24.5	0.14	1450	14300	1.4	10200
17	Polyethylene	3200	40	*	3200**	0.125	24.5	0.23	1052	13900	3	4630

As Figure 2.8 show, before gel placement, a Berea core showed an endpoint permeability to oil of 508md at S_{wr} and endpoint permeability to oil of 120md at S_{or}. After placement of a Cr(III)-acetate-HPAM gel, the permeability during brine injection quickly stabilized around 0.17md, indicating a water residual resistance factor of 706 (120/0.17). in contrast, during oil injection after gel placement, the

permeability rose gradually to 105md after 100 pore volume (PV) injected, indicating an oil residual resistance factor of only 4.8 (508/105), and it still hold potential to decrease.

A second experiment in Figure 2.9 illustrates similar trends in polyethylene core which had no residual oil saturation before gel placement. The core originally had a permeability of 8100md. After same gel placement, the permeability during brine injection quickly stabilized at 60µd indicating a water residual resistance factor of 135000 (8100/0.06). With continuous applied pressure gradient of 30 psi/ft. in contrast, during subsequent oil injection, permeability to oil rose gradually to 1700md over the course of 10000PV.

S. Ganguly et al 2003 also support the ideal that gel dehydration could explain the DPR effect. This experiment has been done by using Berea Sandstone core with permeability around 500md. The experiment use gelant of Alcoflood 935 with 73 cp viscosity at a shear rate of 11.25 sec^{-1} and the nominal gel time was 36 hours. Pressure gradient changed from 40 psi/ft to 174psi/ft.

Table 2.19. Summary of Data Core 2 (S. Ganguly et al 2003)

Run #	Description	Sw (%)	Sgel (%)	Øe (%)	Sw* (%)	So* (%)	Kw (md)	Frrw	Ko	Frro
2.1	pre-treatment Brine Flood 1	100	0	24	100	0	500			
2.2	Oil flood	20	0	24	20	0			525	
2.3	Brine flood 2	74	0	24	74	0	85			
2.4	Gel Injection	0	74	0	0	0	0			
2.5	Oil flood @ 40psi/ft	0	58	8	0	100			38	13.8
2.6	Brine flood 1 @40psi/ft	16	58	9	42	58	0.7	121		
2.7	Oil flood @ 40psi/ft	0	58	9	1	99			64	8.2
2.8	Oil flood @174 psi/ft	0	51	11	1	99			255	2.06
2.9	Brine flood @ 174 psi/ft	30	51	11	64	36	7	12.1		
2.1	Oil flood @ 174 psi/ft	3	51	11	6	94			258	2.03

Table 2.20. Summary of Data Core 3 (S. Ganguly et al 2003)

Run #	Description	Sw (%)	Sgel (%)	Øe (%)	Sw* (%)	So* (%)	Kw (md)	Frrw	Ko (md)	Frro
3.1	pre-treatment Brine Flood 1	100	0	24	1	0	500			
3.2	Oil flood	24	0	24	0	1			500	
3.3	Brine flood 2	72	0	24	1	0	85			
3.4	Gel Injection Brine flood@40 psi/ft	0	72	0	0	1	3.8	23		
3.5	Oil flood @ 40psi/ft	0	50	12	0	1			65	8
3.6	Brine flood 1 @40psi/ft	20	50	12	1	0	1.4	59		
3.7	Brine flood @174 psi/ft	32	40	15	1	0	1.7	49		
3.8	Oil flood @174 psi/ft	0	40	15	0	1			264	2.00
3.9	Brine flood @ 174 psi/ft	31	40	15	1	0	19	4.47		

Table 2.21. Summary of Data Core 4 (S. Ganguly et al 2003)

Run #	Description	Sw (%)	Sgel (%)	So (%)	K (md)	RRF
4.1	Pre treatment Brine flood 1	100	0	0	500	
4.2	Oil flood	27	0	73	506	
4.3	Brine flood 2	72	0	28	88	
4.4	gel injection	0	72	28	0	
4.5	oil flood Dehydration @ 40 psi/ft	0	52	48	123	4.1
4.6	Brine flood at 40 psi/ft	21	52	27	8.7	10.1

Table 2.22. Summary of Data Core 5 (S. Ganguly et al 2003)

Run #	Description	Sw (%)	Sgel (%)	So (%)	K (md)	RRF
5.1	Pre treatment Brine flood 1	100	0	0	484	
5.2	Oil flood	27	0	73	477	
5.3	Brine flood 2	73	0	27	62	
5.4	gel injection	0	72	27	0	
5.5	Brine flood Dehydration @ 40 psi/ft	0	52	27	6.3	9.8
5.6	oil flood at 40 psi/ft	0	47	53	166	2.9
5.7	Brine flood @ 40psi/ft	23	47	31	11	5.6

From the data Table 2.19-2.22, as gels formed within the Berea sandstone, rocks were dehydrated by injection of oil or water, creating a “new” pore channel within the rock-gel system, with the increasing pressure gradient during the dehydration process, the volume of new pore channel will increase due to part of the residual oil saturation reconnected. In addition, pressure gradient had a much larger effect on water permeability than on oil permeability. The large DPR values observed

at the lower range of pressure gradients are attributed to relatively large residual oil saturation in the new pore space and the extremely water-wet nature of the new pore space.

2.4.5 Balance between Capillary Forces and Gel Elasticity. As illustrated in Figure 2.10 when an oil droplet extrudes through an water Based-gel, there are two opposing forces act on it and it cause two effect, a capillary force acts to maintain a minimum droplet radius, which in turn forces open a channel through the gel. On the other side, the gel exerts an elastic confining force to close the channel. The final radius of the oil droplet and the size of the oil pathway depend on the balance between the two forces. Thus the effective permeability to oil increases with increasing radius of the flow path around the oil droplet. In contrast, when water flows through the same channel, no capillary force acts to open the channel because miscible effect. Therefore, the effective permeability to water should be smaller than that to oil. (Dawe and Zhang 1994)

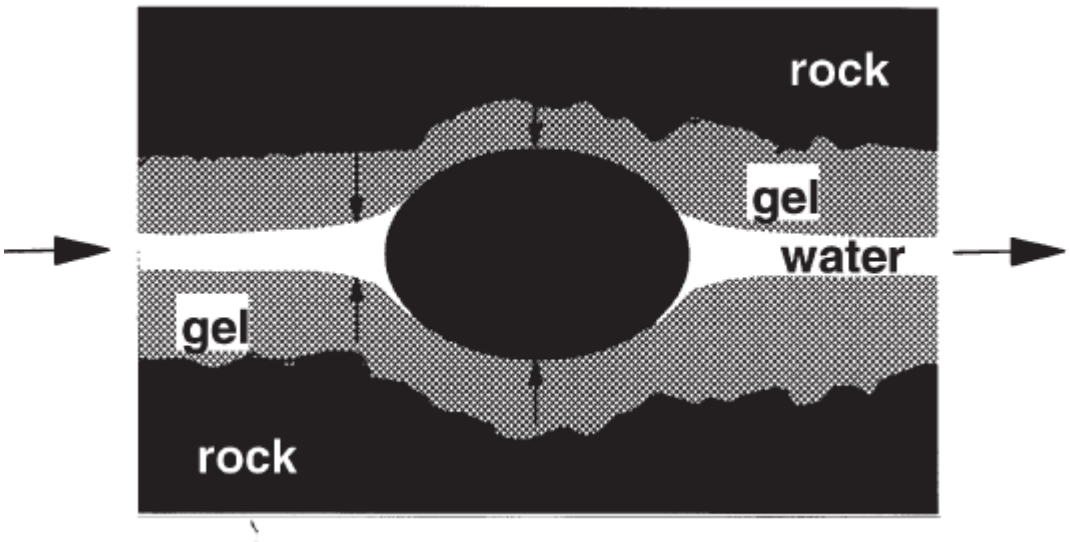

Figure 2.10. Balance between Capillary Forces and Gel Elasticity When Forcing Oil or Water through Water-Based Gel (Dawe And Zhang 1994)

For an oil droplet in water, the capillary pressure across the interface is proportional to the interfacial tension (IFT) divided by the oil droplet radius

$P_C = \frac{2\sigma\ cos\theta}{r}$ for capillary tubes. With weaker capillary force at a given elastic force from the gel, the radius of the flow channel around the oil droplet is reduced. Therefore, if this theory is valid, the DPR should become less prominent if the oil/water interfacial tension is reduced. To test this theory, Seright et al 1997 run the experiment in glass conduits using an oil soluble surfactant to lower the oil/water interfacial tension. The addition of 0.1% surfactant to the oil phase lowered the oil/water interfacial tension from 42.5dyne/cm to 8dyne/cm in 1% NACL brine at 41°C. Results showed that the permeability to oil was more than twice greater in the absence of surfactant than in the presence of 0.1% surfactant which supports this mechanism. However weather the behavior observed in glass conduits is representative of the behavior in cores is still left unknown.

To further test this theory, increasing gel elasticity should allow the capillary force to open a large path around the oil droplet, resulting in a higher effective permeability to oil. Another possible way is to quench the gelation reaction at different stages of the gelation process (Liang and R.S. Seright 2002). Hydroquinone-hexamethylenete-tramine-HPAM have been used which requires high temperatures for the gelation reaction to process at a significant rate. Using aged gelant at 110°C, followed by quenching to 41°C. Two experiments were performed in high permeability Berea sandstone cores. In both cases, 10 pore volumes (PV) of the gelant were injected into the core at room temperature (26°C). For the first oil/water experiment, the core was shut in at 110°C for 2 days, after two day shut in period, the temperature was lowered to 41°C to quench the gelation reaction. For the second oil/water experiment, the core was shut in at 110°C for 8 days before lowering the

temperature to 41°C. The gel with gelation reaction quenched after 8 days should be less elastic than 2 days gelation.

Table 2.23. Frrw and Frro Values for HPAM Gel in Berea Sandstone (Liang and R.S. Seright 2002)

Frrw and Frro values for a HPAM gel in berea sandstone							
Days	Kw (md)	First Frro	First Frrw	Second Frro	Second Frrw	First Frro/Frrw	Second Frro/Frrw
2	467	20	4.7	20	4.2	4.25	4.76
8	286	13.6	10.2	14.6	8.7	1.33	1.68

From the Table 2.23, surprisingly, the two day gel reduced the permeability to oil significantly more than to water. The DPR was less pronounced for the less-elastic 8 day gel which did not support the elasticity theory.

Hamed. H et al 1999 clarify the mechanism of the balance between capillary force and gel elasticity by using visualization and quantification methods. Flow experiments were conducted in bulk, single pore channels, and porous glass micro-models. The gelant used was polyacrylamide-chromium acetate. The results show that polymer gels reduce water permeability more than oil permeability which imply that the flow characteristic were controlled by the elasticity of polymer gels. The DPR is a characteristic of the polymer gel and the porous media, so different polymer systems may have different DPR mechanisms which indicate the pore size distribution, the end-point saturations before treatment and the gelant concentration are the controlling parameters for DPR.

2.4.6 Gravity Effects. It demonstrate that gravity influence the location of gel particles in pores. For a water-based gel, the density of the gel is similar to the brine. During water flooding, gel particles floating freely in the water phase can be easily

caught in the pore throats, thereby reducing water permeability. However, during oil flooding, we assume if the fluid velocity is low enough, the density difference between the water-based gel particles and the oil could cause the gel particles to settle away from the pore throats, thereby allowing higher permeability for oil. (Liang, R.S Seright 1995)

Berea sandstone cores with high absolute permeability have been used to do experiments. Results showed that the Frrw and Frro values were not sensitive to flow direction or core orientation, through the water/oil injection cycles, the gel consistently reduced water permeability more than oil permeability, which suggests that the DPR was not caused by gravity effect.

2.4.7 Lubrication Effect. For water-wet cores where a layer of polymer or gel is adsorbed onto pore walls, the presence of adsorbed polymer interface effectively lubricates the flow of oil or gas through the center of pores (Sparlin.D, Hagen, R.W 1984. Zaitoun, et al 1988) If this theory is valid the residual resistance factors should vary with oil viscosity during core experiments with gel present. Therefore, experiment has been done by using a strongly water-wet Berea sandstone core and two oils (oil A and oil B) with different viscosities at constant temperature (Liang J and Seright. R.S 1994). Table 2.24 provides average endpoint permeability value for the different fluids. If a lubrication effect was important, the apparent oil permeability should have been much greater for oil B than for oil A.

Table 2.24. Effect of Oil Viscosity on Endpoint Permeability before Gel Treatment (Liang J and Seright. R.S 1994)

oil	μo (cp)	Swr	Ko (md)	Swr*	Ko* (md)
A	1.05	0.28	503	0.26	522
B	31.6	0.24	561	0.23	588
A	1.05	0.24	537	0.23	561
	μw (cp)	Sor	Kw(md)	Sor*	Kw* (md)
	0.67	0.34	112	0.35	124
Brine; 1% Nacl					
All test done in strongly water-wet Berea sandstone core at 105°F					
* flow direction reversed					

Table 2.25. Effect of Oil Viscosity on Frr (Liang J and Seright. R.S 1994)

Fluid injected	Sw+Sgel	Sor	Frro	Frrw
1% Nacl brine		0.35		>35,000
Oil A	0.5		50	
Oil B	0.46		20	
Oil A	0.46		20	
Oil B	0.43		10	
Oil A	0.43		10	
1% Nacl brine		0.44		1430×U E(-0.44)
Gelant; 1.39% HPAM/0.0212% Cr(III) acetate				
Oil A; μ_o=1.05cp, ρ_o=0.76g/cm3				
Oil B; μ_o=31.6cp and ρ_o=0.88g/cm3				
All test run at 105°C				

From Table 2.25 at a given saturation, the F_{rro} values for the two oils were essentially the same and the F_{rro} values did not vary with oil viscosity which suggests no lubrication effect was apparent. The decreased F_{rro} in the repeated experiment may cause by gel breakdown which is not the reason for disproportionate permeability reduction.

2.4.8 Wettability Effect. Zaitoun and Kohler 1989 proposed that in a strongly water wet system; the presence of residual oil droplets at the center of the pores can significantly reduce the effective pore radius during water flooding. In contrast, no such constriction exists during oil flooding. We expect the strongly water wet surface is more easily for water flow than intermediate wetting surface. The experiment has been done by using both strongly water wet cores and cores of intermediate wettability. (Liang, J. Sun, H and Seright, R.S 1992).

Table 2.26. Wettability Effect on Gel Performance (Liang, J. Sun, H and Seright, R.S 1992)

Gelant	core wettability	Frrw	Frro	Frrw/Frro
3% resorcinol/3%formaldehyde	strongly water wet	49	11	4.5
	intermediate	510	26	20
0.4% Xanthan/0.0154%Cr(III)	strongly water wet	8	5	1.6
	intermediate	22	14	1.6

Table 2.26 shows the DPR was observed in systems of intermediate wettability as well as in strongly water wet systems. From the data, for the first gel, the DPR was actually more evident in a core of intermediate wettability than in a strongly water wet core. For the second gel, wettability on DPR effect was not evident. Obviously, the effect of wettability on gel performance varied with the gel.

To further verify how wettability influence the DPR. Experiment has been settled (Ph. Elmkies, H. Bertin,et al 2002), in order to get different wettability at the same core. Wettability modification was obtained by aging the core saturated with crude oil at irreducible water saturation at temperature of 60℃ for 6 weeks. The nonionic polyacrylamide solution was prepared at a concentration of 2500 ppm, for each experiment, two types of carbonate rocks were used in these experiments. The first one was St-Maximin limestone referred to as “StMax” with a porosity of 0.43

and second one was an Estaillades limestone. The Estaillades cores had a porosity ranging from 0.19 to 0.236.

Table 2.27. Wettability Effect on Disproportionate Permeability Reduction (Ph. Elmkies, H. Bertin,et al 2002)

Core sample	Oil permeability reduction(Rko)	Water permeability reduction (Rkw)
water-wet "StMax"	1.4	2.25
Wettability-modified "St Max"	1.03	1.52
water-wet 'Estaill"	1.64	3
Wettability-modified "Wstaill"	1.3	1.75
water-wet "Estail2"	1.3	5.2
wettability-modified "Estail2"	1.3	2.64

From Table 2.27, the results show a selective effect of adsorbed polymer on all the cores, the adsorbed polymer did not strongly affect oil permeability since R_{ko} (oil permeability reduction) values are ranging from 1.03 to 1.64. However, it reduced water permeability by a factor ranging from 1.52 to 5.2. When wettability of the core is modified, making the core less water wet, water permeability reduction decreases slightly which suggests the DPR effect is enhanced in water-wet core than mix-wet core.

However, most of the proposed DPR mechanisms are based on the experimental results of oil/water systems. Only a few of them are based on gas/water system. Zaitoun and his co-workers attributed the DPR in water and gas to the wall effect (Zaitoun and Kohler 1989; Zaitoun 1991). DPR mechanisms have been argued for long time due to different core models and experimental design used by different researchers. Moreover, all the previous experiments were performed either in consolidated cores, sand-packed cores or visual pore-networked micro models. Other than core fracture models, In our work, we fabricated three shale fracture models with

different fracture width and set up a core flooding apparatus to conduct brine/gas injection experiments before and after polymer treatment. A method by which to calculate the residual resistance factor for gas (Frrg) was defined. The effect of polymer on water/gas flow behavior in the microfractures of shale reservoirs was discussed, and the mechanisms responsible for disproportionate permeability reduction in the fractured shales were proposed.

3. EXPERIMENTS

3.1. MATERIALS

Cylindrical shale cores with a diameter of 1 inch and a length of 2 inches were used to fabricate shale fracture models. As Figure 3.1 depicts, each shale core was cut in half from the center, and stainless steel sheets with different thicknesses (Maudlin Products, Kemah, TX) were inserted between the two halves to model fractures. The fracture height of all the shale fracture models was 0.54 cm, and the fracture widths were 0.002 inches, 0.003 inches and 0.004 inches, respectively. The shale cores were used in the experiments because they could better model the adsorption-entanglement effect of polymer on fracture surfaces.

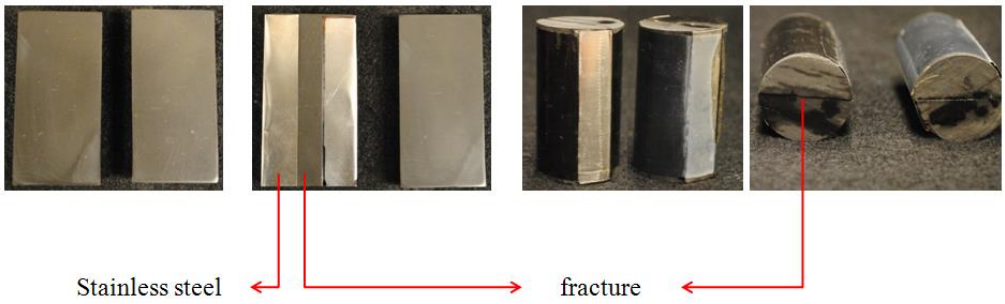

Figure 3.1. Shale Fracture Models Used in the Experiment

In this experiment, brine was made from sodium chloride (NaCl) and distilled water with a NaCl weight percentage of 2%, a density of 1.02 g/cm^3 and a viscosity of 1.03 mPa·s. The gas was pure nitrogen with a density of 1.36×10^{-3} g/cm^3 and a viscosity of 0.0178 mPa·s at standard temperature and pressure conditions. A commercial polyacrylamide-based polymer (SNF, Riceboro, GA) was used to prepare a 0.1 wt% polymer solution exhibiting a high molecular weight and medium to high anionicity.

3.2. EXPERIMENTAL SETUP

Figure 3.2 presents the flow chart of the experimental setup composed of a power driving system, a core holder, a data measurement system and a data acquisition system. The power driving system contained an ISCO 500D syringe pump A (Teledyne Technologies, Thousand Oaks, CA) and a compressed nitrogen cylinder for brine and gas injection, respectively. An ISCO 500D syringe pump B provided the confining pressure for the core holder. A ProSense pressure sensor (AutomationDirect, Cumming, GA) with a range of 0 ~ 100 in H_2O or 0 ~ 15 psi was installed in the inlet of the core holder to measure the real-time injection pressure. During gas-injection experiments, a gas flow meter (OMEGA Engineering, Stamford, CT) with a range of 0 ~ 1000 Scm^3/min was installed in the inlet of the core holder to measure the gas flow rate in real time. RHINO power (AutomationDirect, Cumming, GA) and a myPCLab data logger (Novus Automation, Porto Alegre, Brazil) were included in the data acquisition system to enable the fluid injection pressure and gas flow rate to be displayed and recorded on the computer. The outlet pressure of the core holder during the experiments was the atmospheric pressure.

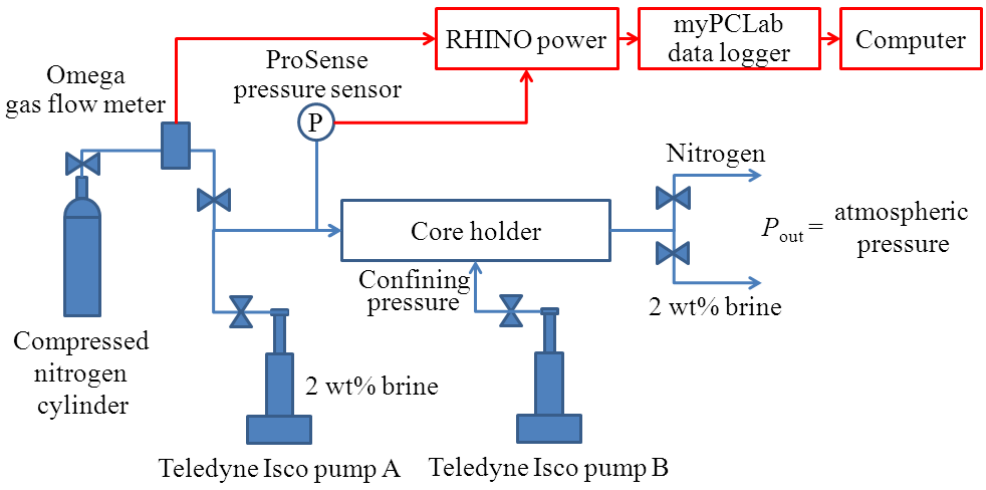

Figure 3.2. Diagram of Shale Fracture Model Experimental Setup

3.3. EXPERIMENTAL PROCEDURE

Figure 3.3 depicts the experimental sequence during the core flooding experiments which is explained as follows. Noted that the flow of gas, brine and polymer solution in the matrix was negligible, and the fracture served as the only flow path due to the ultra-low permeability of the shale matrix.

① The shale cores were put into the oven for 12 hours, vacuumed for another 12 hours and then immersed in 2 wt% NaCl brine for another 12 hours.

② Shale fracture models were fabricated and employed in the core holder. The confining pressure was set at 400 psi.

③ Nitrogen was injected to displace brine until reaching residual water saturation conditions in the fracture.

④ Brine was used to displace gas until reaching residual gas saturation conditions in the fracture, and then injected at different flow rates (from the lowest to the highest) to measure the stable injection pressures at residual gas saturation in the fracture.

⑤ Polymer solution was injected at a constant flow rate of 0.1 cm^3/min for 12 hours.

⑥ Brine was injected at different flow rates in sequence (from the lowest to the highest in the first cycle, and from the highest to the lowest in the second cycle) to measure the stable injection pressures at residual gas saturation in the fracture.

⑦ The shale core surfaces were polished to get absorbed polymer layers cleaned, and then another shale fracture model was fabricated to repeat step ① ~ step ③.

⑧ Gas was injected at different flow rates (from the highest to the lowest) to measure the stable injection pressures at residual water saturation in the fracture.

⑨ Step ⑤ was repeated.

⑩ Gas was injected at different flow rates in sequence (from the lowest to the highest in the first cycle, and from the highest to the lowest in the second cycle) to measure the stable injection pressures at residual water saturation in the fracture.

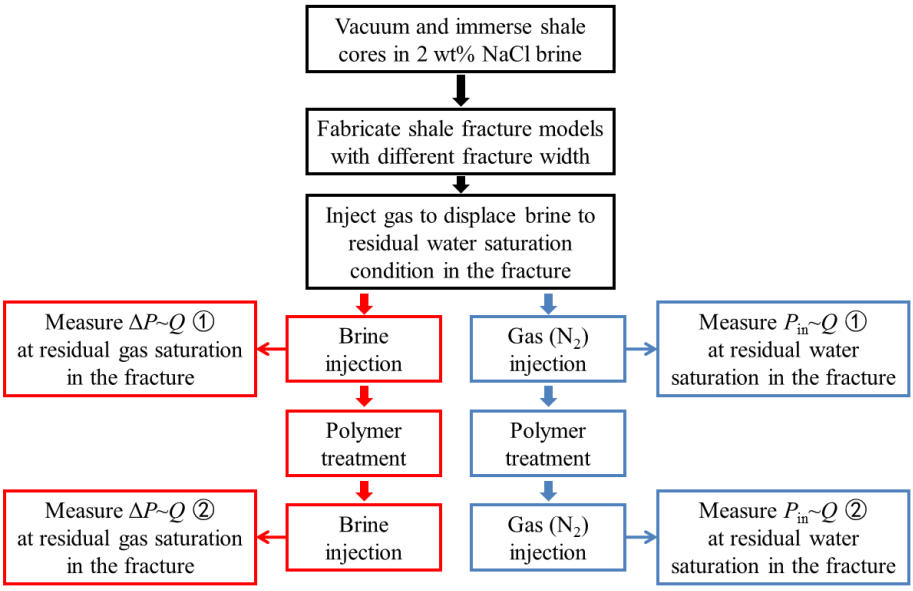

Figure 3.3. Flow Chart of Experimental Procedure

4. METHODOLOGY

4.1. RESIDUAL RESISTANCE FACTOR FOR WATER

Newtonian fluid flow through porous media follows Darcy's law, as follows:

$$Q = \frac{k k_{\mathrm{w}} A}{\mu_{\mathrm{w}} L}(P_{\mathrm{in}} - P_{\mathrm{out}}) \tag{1}$$

where Q is the water flow rate; k is the absolute permeability; k_{w} is the relative permeability of the water phase; μ_{w} is the water viscosity; A is the sectional area of the shale fracture model; L is the length of the shale fracture model; and $P_{\mathrm{in}} - P_{\mathrm{out}}$ is the differential pressure across the fractured shale..

The residual resistance factor for brine ($F_{\mathrm{rr,water}}$) refers to the reduction in the permeability of the water phase caused by the polymer treatment. It is calculated by dividing the permeability of the water phase before the polymer treatment by the permeability of the water phase after the polymer treatment at the same brine injection rate. According to Eq. (1), the residual resistance factor can be computed by dividing the brine-injection pressure drop after the polymer treatment by the brine-injection pressure drop before the polymer treatment at the same brine injection rate, as follows:

$$F_{\mathrm{rr,water}} = \frac{k_{\mathrm{b}}}{k_{\mathrm{a}}} = \left.\frac{\Delta P_{\mathrm{a}}}{\Delta P_{\mathrm{b}}}\right|_{Q} \tag{2}$$

where $F_{\mathrm{rr,water}}$ is the residual resistance factor for brine; k_{b} is the permeability of the water phase before the polymer treatment; k_{a} is the permeability of the water phase after the polymer treatment; ΔP_{a} is the brine-injection pressure drop after the

polymer treatment; and ΔP_b is the brine-injection pressure drop before the polymer treatment.

During the brine-injection experiments, 12 superficial velocities (Table 4.1) were designed for each shale facture model. However, due to the range limit of the pressure sensors, not all brine-injection pressures were obtained at different superficial velocities. Taking the shale fracture model with a fracture width of 0.002 inches as an example, brine-injection pressures were recorded at superficial velocities of 0.05 m/s to 1.5 m/s before the polymer treatment. According to the experimental procedures noted in section 3.3 and Eq. (2), the $F_{rr,water}$ can be obtained at different water flow rates and corresponding shear rates.

Table 4.1. Water Flow Rate and Shear Rate Designed in Brine-injection Experiments

Superficial velocity (m/s)	Water flow rate (cm^3/s)			Shear rate (s^{-1})		
	W_f = 0.002 inches	W_f = 0.003 inches	W_f = 0.004 inches	W_f = 0.002 inches	W_f = 0.003 inches	W_f = 0.004 inches
0.05	0.014	0.021	0.027	984.25	656.17	492.13
0.1	0.027	0.041	0.055	1968.50	1312.34	984.25
0.15	0.041	0.062	0.082	2952.76	1968.50	1476.38
0.2	0.055	0.082	0.110	3937.01	2624.67	1968.50
0.25	0.069	0.103	0.137	4921.26	3280.84	2460.63
0.3	0.082	0.123	0.165	5905.51	3937.01	2952.76
0.5	0.137	0.206	0.274	9842.52	6561.68	4921.26
1	0.274	0.411	0.549	19685.04	13123.36	9842.52
1.5	0.411	0.617	0.823	29527.56	19685.04	14763.78
2	0.549	0.823	1.097	39370.08	26246.72	19685.04
2.5	0.686	1.029	1.372	49212.60	32808.40	24606.30
3	0.823	1.234	1.646	59055.12	39370.08	29527.56

4.2. RESIDUAL RESISTANCE FACTOR FOR GAS

The Darcy's law equation for gas flow through porous media can be expressed as:

$$Q_{gsc} = \frac{k k_{rgas} A}{2 \mu_g L} \frac{P_{in}^2 - P_{out}^2}{P_{base}} \tag{3}$$

where Q_{gsc} is the gas flow rate at the condition of P_{base}; k_{rgas} is the relative permeability of the gas phase; μ_g is the gas viscosity at the condition of P_{base}; P_{base} is the base pressure; and $P_{base} = P_{out}$ is the atmospheric pressure in this case.

According to the definition of a residual resistance factor and Eq. (3), the residual resistance factor for gas ($F_{rr,gas}$) was derived as:

$$F_{rr,gas} = \frac{k_b}{k_a} = \left[\left(\frac{P_{in}^2 - P_{out}^2}{P_b}\right)_{after} / \left(\frac{P_{in}^2 - P_{out}^2}{P_b}\right)_{before}\right]\Bigg|_{Q_{gsc}} \quad (4)$$

During the gas-injection experiments, six superficial velocities (Table 4.2) were designed for each shale fracture model. Because compressed nitrogen cylinder was controlled through a regulator, it cannot be set precisely at a gas flow rate without a mass flow controller. Therefore, a new approach was developed to determine the $F_{rr,gas}$:

① Gas flow rates (i.e., $Q_1 \sim Q_6$) were calculated at different superficial gas velocities (i.e., $V_1 \sim V_6$) in Table 4.2.

② Two observation points (e.g., Q_{1a} and Q_{1b}) were added for each gas flow rate (e.g., Q_1). The regulator of the compressed nitrogen cylinder was operated to set gas flow rates as close as three observation points (i.e., Q_{1a}, Q_1 and Q_{1b}). The stable gas-injection pressures P_{in} were measured and recorded.

③ The binomial equation between $(P_{in}^2\text{-}P_{out}^2)/P_{base}$ and Q_{gsc} was fitted based on the data collected from the three observation points for each gas flow rate (e.g., Q_1).

④ Substituting the gas flow rate (e.g., Q_1) allows the corresponding $[(P_{in}^2\text{-}P_{out}^2)/P_{base}]_{before}$ to be obtained.

⑤ After the polymer treatment, step ② ~ step ④ were repeated to obtain the corresponding $[(P_{in}^2-P_{out}^2)/P_{base}]_{after}$ at the gas flow rate (e.g., Q_1).

⑥ Eq. (4) was used to obtain the $F_{rr,gas}$ at different gas flow rates and their corresponding superficial velocities.

Table 4.2. Superficial Gas Velocity and Gas Flow Rate Designed in Gas-injection Experiments

Superficial gas velocity (m/s)	Gas flow rate (Scm^3/s)			
	Q	W_f = 0.002 inches	W_f = 0.003 inches	W_f = 0.004 inches
V_1 = 5	Q_{1a}	0.955	1.391	1.827
	Q_1	1.372	2.057	2.743
	Q_{1b}	1.788	2.724	3.660
V_2 = 10	Q_{2a}	2.327	3.448	4.570
	Q_2	2.743	4.115	5.486
	Q_{2b}	3.160	4.781	6.403
V_3 = 15	Q_{3a}	3.698	5.506	7.313
	Q_3	4.115	6.172	8.230
	Q_{3b}	4.531	6.839	9.146
V_4 = 20	Q_{4a}	5.070	7.563	10.056
	Q_4	5.486	8.230	10.973
	Q_{4b}	5.903	8.896	11.889
V_5 = 25	Q_{5a}	6.441	9.620	12.799
	Q_5	6.858	10.287	13.716
	Q_{5b}	7.275	10.954	14.633
V_6 = 30	Q_{6a}	7.813	11.678	15.543
	Q_6	8.230	12.344	16.459
	Q_{6b}	8.646	13.011	16.793

5. RESULTS AND DISCUSSION

5.1. EFFECT OF POLYMER ON WATER FLOW BEHAVIOR

As Figures 5.1, 5.2 and 5.3 illustrate, before the polymer treatment and in the first cycle after the polymer treatment, pressure drops at different water flow rates were measured through step ④ and step ⑥ in section 3.3. These data show similar trends for the three shale fracture models with different fracture widths.

Before the polymer treatment, the linear equations between the pressure drop and water flow rate were fitted with good agreement for the three shale fracture models at low water flow rates. However, the second straight lines were observed with a break point before Q = 0.2 cm^3/s. This is attributed to a saturation change due to the increasing injection rate and the inertial force associated with high flow rates.

Compared to the results before the polymer treatment, the water injection pressure drop in the first cycle after the polymer treatment increased due to the effect of polymer in the fractures (Figure 5.4).

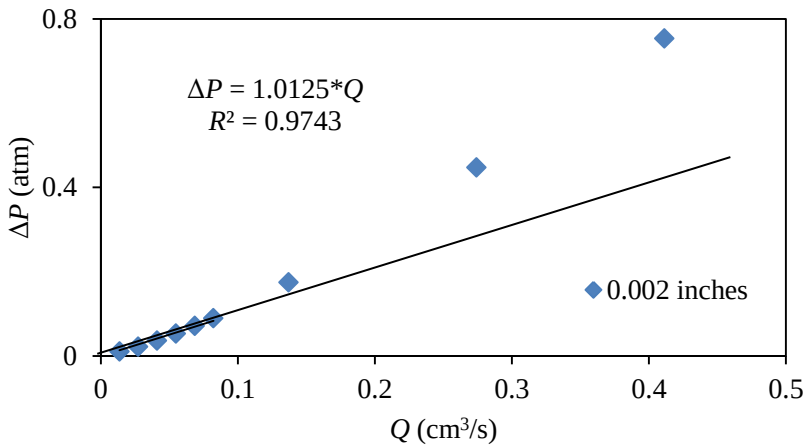

Figure 5.1. Relationship between ΔP and Q for Shale Fracture Model with a Fracture Width of 0.002 inches

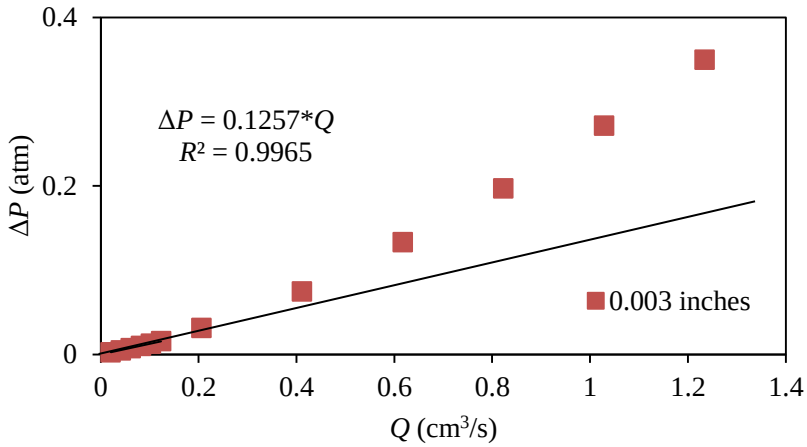

Figure 5.2. Relationship between Δ*P* and *Q* for Shale Fracture Model with a Fracture Width of 0.003 inches

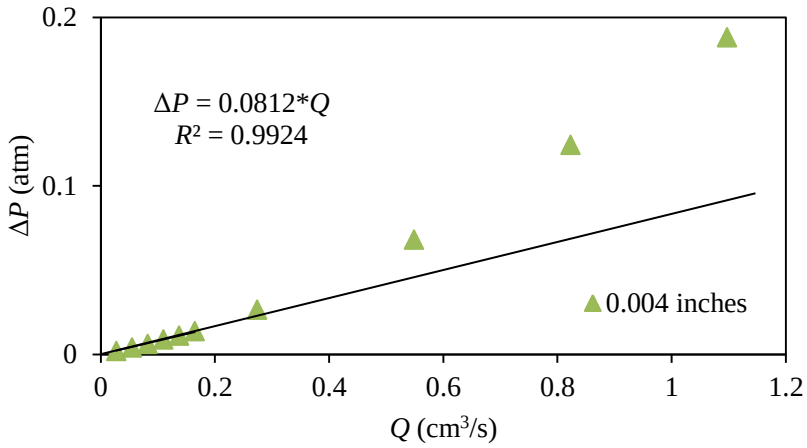

Figure 5.3. Relationship between Δ*P* and *Q* for Shale Fracture Model with a Fracture Width of 0.004 inches

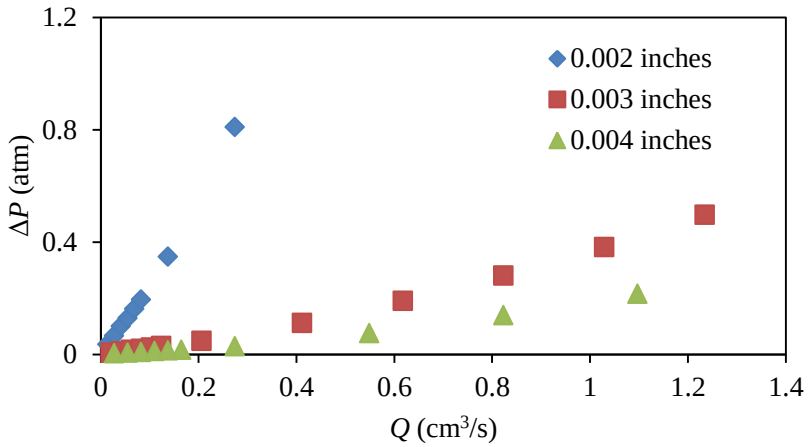

Figure 5.4. Relationship between Δ*P* and *Q* in the First Cycle after the Polymer Treatment

According to the pressure drops before and after the polymer treatment, Eq. (2) was used to calculate $F_{rr,water}$ at different shear rates, as shown in Figures 5.5, 5.6 and 5.7 respectively. The three figures show similar trends.

In the first cycle after the polymer treatment, the $F_{rr,water}$ decreased as the shear rate increased at low water flow rates. One reason for this decrease could be that the brine flushed more and more polymer out of the shale fracture models as the water flow rate (i.e., shear rate) increased. Another reason could be that the polymer coating the fracture surfaces was squeezed more at higher flow rates due to its elasticity and deformability. Therefore, the water flow channels became larger, and the resistance of the polymer to water flow decreased. Eventually, brine could flow primarily through channels formed at the very beginning, and no new channels would form even if the flow rate continued to increase. Hence, the $F_{rr,water}$ tends to stabilize at high shear rates.

For the same shale fracture model, the $F_{rr,water}$ was smaller in the second cycle than in the first cycle at the same shear rate because some polymer was flushed out in the first cycle, and the remaining polymer could not be flushed any more.

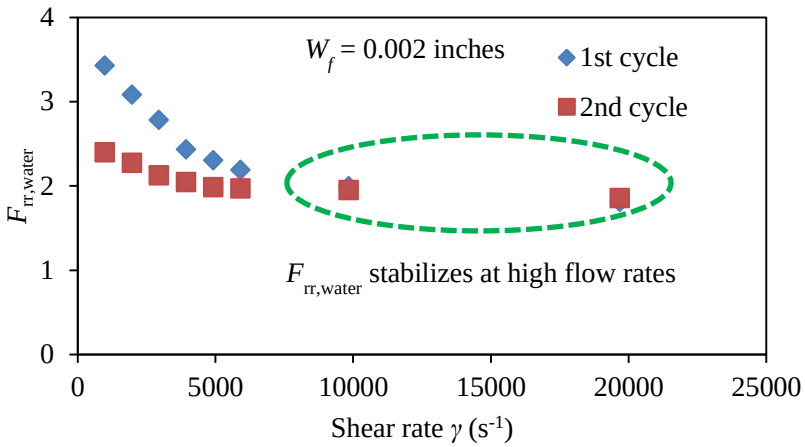

Figure 5.5. Relationship between $F_{rr,water}$ and γ for Shale Fracture Model with a Fracture Width of 0.002 inches

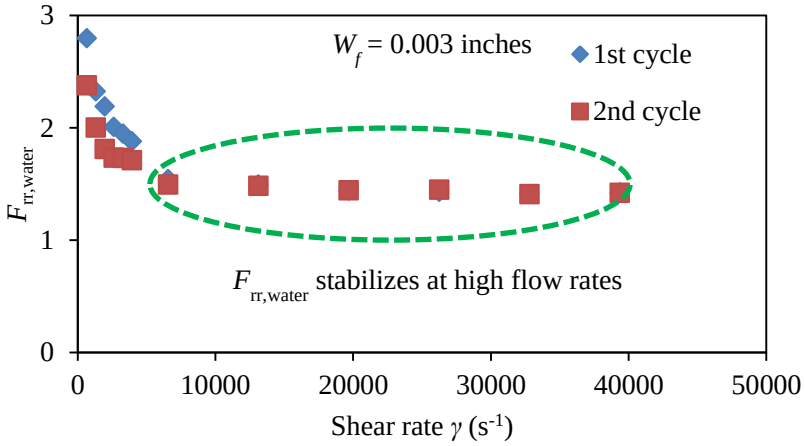

Figure 5.6. Relationship between $F_{rr,water}$ and γ for Shale Fracture Model with a Fracture Width of 0.003 inches

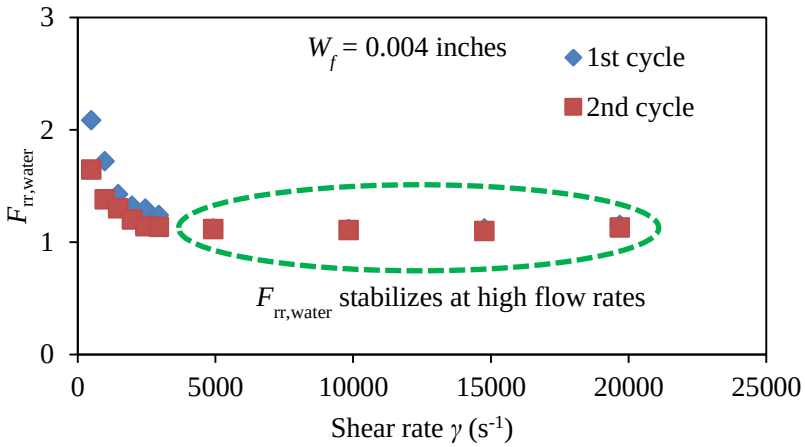

Figure 5.7. Relationship between $F_{rr,water}$ and γ for Shale Fracture Model with a Fracture Width of 0.004 inches

Figures 5.8 and 5.9 show $F_{rr,water}$ for all fracture widths as a function of shear rate on a log-log scale. In both the first and second cycles, the relationship between the $F_{rr,water}$ and the shear rate can be fitted well using a power-law equation, as follows:

$$F_{rr,water} = \alpha \gamma^{m} \tag{5}$$

where α and m are coefficients related to the experimental conditions; and γ is the shear rate, s^{-1}.

Table 5.1 lists the coefficients of fitting equation and correlation factors in the two cycles for the three shale fracture models. The agreement was good for all of the equations.

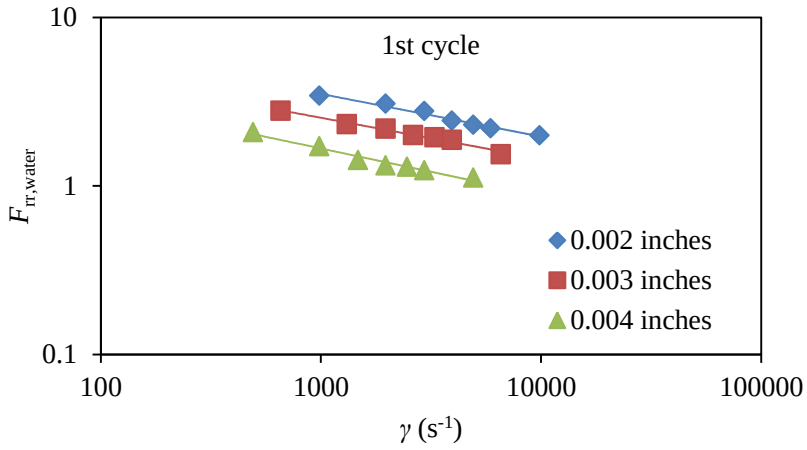

Figure 5.8. Comparison of $F_{rr,water}$ at Different Fracture Widths in the First Cycle after the Polymer Treatment

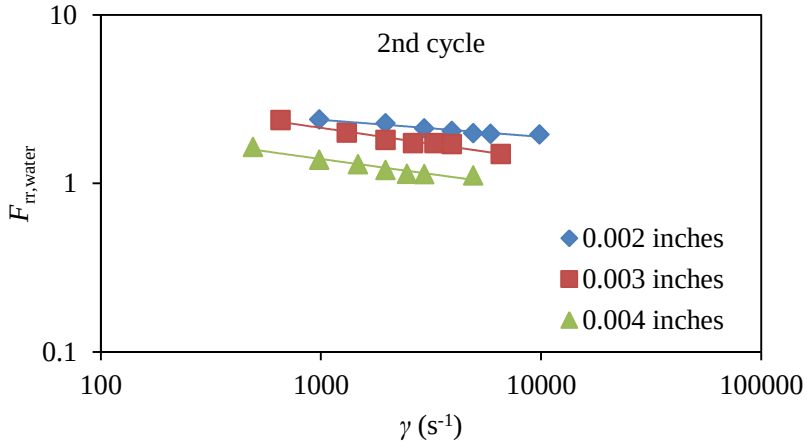

Figure 5.9. Comparison of $F_{rr,water}$ at Different Fracture Widths in the Second Cycle after the Polymer Treatment

Table 5.1. Coefficients of Fitting Equation for $F_{rr,water}$ as a Function of Shear Rate

Fracture width (inches)	Cycle	Coefficient of fitting equation		R^2
		α	m	
0.002	1st cycle	20.228	-0.253	0.9756
	2nd cycle	4.805	-0.101	0.9407
0.003	1st cycle	13.619	-0.243	0.9804
	2nd cycle	7.881	-0.189	0.9643
0.004	1st cycle	11.252	-0.276	0.9711
	2nd cycle	4.810	-0.179	0.9333

Figures 5.8 and 5.9 show that the $F_{rr,water}$ was smaller in wider fractures at the same shear rate. This finding is reasonable because the thickness of the remaining polymer layer relative to a wide fracture is much thinner than that to narrow fractures. During polymer injection, superficial polymer velocity is lower in a wider fracture at the same polymer injection rate. Therefore, polymer bridging effect weakens and polymer exhibits lower resistance to water flow. On the other hand, polymer flow capability is greater in a wider fracture. Hence, more polymers were flushed out during brine injection and the remaining polymer layer is thinner in a wider fracture.

5.2. EFFECT OF POLYMER ON GAS FLOW BEHAVIOR

According to the residual resistance factor for gas ($F_{rr,gas}$), gas-injection pressures P_{in} at different gas flow rates Q_{gsc} were recorded through step ⑧ in section 3.3 for the three shale fracture models with different fracture widths. The relationship between $(P_{in}^2-P_{out}^2)/P_{base}$ and Q_{gsc} are plotted in Figure 5.10. The gas permeability increases with increasing average pressure (i.e., the mean pressure between inlet and outlet pressures), which is referred to Klinkenberg effect. Therefore, according to Eq.

(3), the $(P_{in}^2-P_{out}^2)/P_{base}$ was not expected to be linear with the gas flow rates in Figure 5.10. As the fracture width increased, the gas-injection pressure P_{in} and $(P_{in}^2-P_{out}^2)/P_{base}$ decreased. This relationship was attributed to the reduced gas flow resistance in wider fractures.

Based on the new approach for determining the $F_{rr,gas}$, the binomial equation $(P_{in}^2-P_{out}^2)/P_{base}$ can be fitted well as a function of the gas flow rate Q_{gsc} for each superficial velocity (i.e., $V_1 \sim V_6$) in Table 4. 2. Tables 5.2, 5.3 and 5.4 present the fitting equations for the three shale fracture models, respectively. Then, $(P_{in}^2-P_{out}^2)/P_{base}$ before the polymer treatment can be calculated for each gas flow rate Q_{gsc} using these fitting equations.

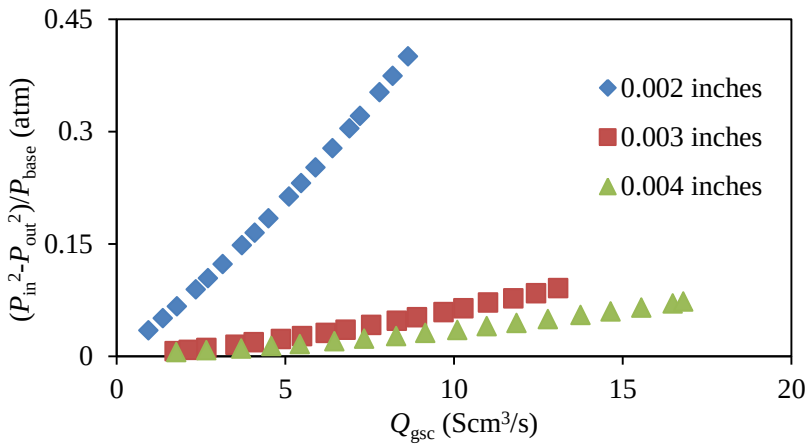

Figure 5.10. Relationship between $(P_{in}^2-P_{out}^2)/P_{base}$ and Q_{gsc} before the Polymer Treatment

Table 5.2. Fitting Equations between $(P_{in}^2-P_{out}^2)/P_{base}$ and Q_{gsc} before the Polymer Treatment for Shale Fracture Model with a Fracture Width of 0.002 inches

Superficial gas velocity (m/s)	Flow rate (Scm^3/s)	Fitting equation $(P_{in}^2-P_{out}^2)/P_{base} = AQ_{gsc}^2 + BQ_{gsc} + C$	$(P_{in}^2-P_{out}^2)/P_{base}$ (atm)
$V_1 = 5$	$Q_1 = 1.372$	A=0.00188427 B=0.03313340 C=0.00161753	0.0506
$V_2 = 10$	$Q_2 = 2.743$	A=0.00171685 B=0.03276323 C=0.00296808	0.1058
$V_3 = 15$	$Q_3 = 4.115$	A=0.00265739 B=0.02397286 C=0.02240391	0.1660
$V_4 = 20$	$Q_4 = 5.486$	A=0.00126622 B=0.03574983 C=-0.00275819	0.2315
$V_5 = 25$	$Q_5 = 6.858$	A=-0.00003135 B=0.05295749 C=-0.05986910	0.3018
$V_6 = 30$	$Q_6 = 8.230$	A=0.00166357 B=0.02911060 C=0.02439842	0.3766

Table 5.3. Fitting Equations between $(P_{in}^2-P_{out}^2)/P_{base}$ and Q_{gsc} before the Polymer Treatment for Shale Fracture Model with a Fracture Width of 0.003 inches

Superficial gas velocity (m/s)	Flow rate (Scm^3/s)	Fitting equation $(P_{in}^2-P_{out}^2)/P_{base} = AQ_{gsc}^2 + BQ_{gsc}+C$	$(P_{in}^2-P_{out}^2)/P_{base}$ (atm)
$V_1 = 5$	$Q_1 = 2.057$	A=0.00009774 B=0.00398311 C=-0.00037206	0.0082
$V_2 = 10$	$Q_2 = 4.115$	A=-0.00099893 B=0.01414130 C=-0.02213273	0.0191
$V_3 = 15$	$Q_3 = 6.172$	A=0.00054457 B=0.00013030 C=0.00944005	0.0310
$V_4 = 20$	$Q_4 = 8.230$	A= 0.00029434 B= 0.00279241 C=0.00373801	0.0467
$V_5 = 25$	$Q_5 = 10.287$	A=0.00082121 B=0.00742392 C=0.05362319	0.0642
$V_6 = 30$	$Q_6 = 12.344$	A= 0.00048375 B=-0.00151135 C=0.02779376	0.0829

Table 5.4. Fitting Equations between $(P_{in}^2-P_{out}^2)/P_{base}$ and Q_{gsc} before the Polymer Treatment for Shale Fracture Model with a Fracture Width of 0.004 inches

Superficial gas velocity (m/s)	Flow rate (Scm^3/s)	Fitting equation $(P_{in}^2-P_{out}^2)/P_{base} = AQ_{gsc}^2 + BQ_{gsc} + C$	$(P_{in}^2-P_{out}^2)/P_{base}$ (atm)
$V_1 = 5$	$Q_1 = 2.743$	A=-0.00013660 B=0.00328020 C=0.00003609	0.0080
$V_2 = 10$	$Q_2 = 5.486$	A=0.00052143 B=-0.00222966 C=0.01268400	0.0161
$V_3 = 15$	$Q_3 = 8.230$	A=0.00076577 B=-0.00834774 C=0.04333428	0.0265
$V_4 = 20$	$Q_4 = 10.973$	A=-0.00049838 B=0.01616063 C=-0.07738596	0.0399
$V_5 = 25$	$Q_5 = 13.716$	A=0.00008176 B=0.00315914 C=-0.00414484	0.0546
$V_6 = 30$	$Q_6 = 16.459$	A=0.00158824 B=-0.04475580 C=0.37645722	0.0701

After the polymer treatment, two cycles of experiments were conducted to measure the gas-injection pressures P_{in} at different gas flow rates Q_{gsc}. Through step ⑩ in section 3.3, the gas flow rates were tested from the lowest to the highest in the first cycle, and from the highest to the lowest in the second cycle. For the two shale fracture models with fracture widths of 0.002 inches and 0.004 inches, a third cycle of experiments in which the gas flow rates were tested from the lowest to the highest was performed to investigate the gas-injection pressure trends.

The comparison of $(P_{in}^2-P_{out}^2)/P_{base}$ before and after the polymer treatment are plotted in Figures 5.11, 5.12 and 5.13 for the three shale fracture models. The pressure response significantly changes with different fracture widths, which results in the change in scale on the y-axis in the figures.

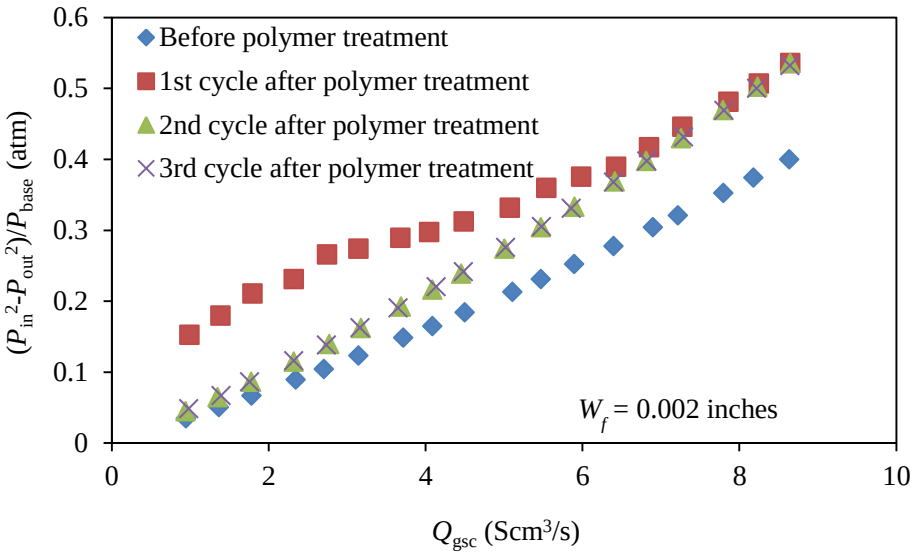

Figure 5.11. Comparison of $(P_{in}^2-P_{out}^2)/P_{base}$ before the Polymer Treatment and after the Polymer Treatment for Shale Fracture Model with a Fracture Width of 0.002 inches

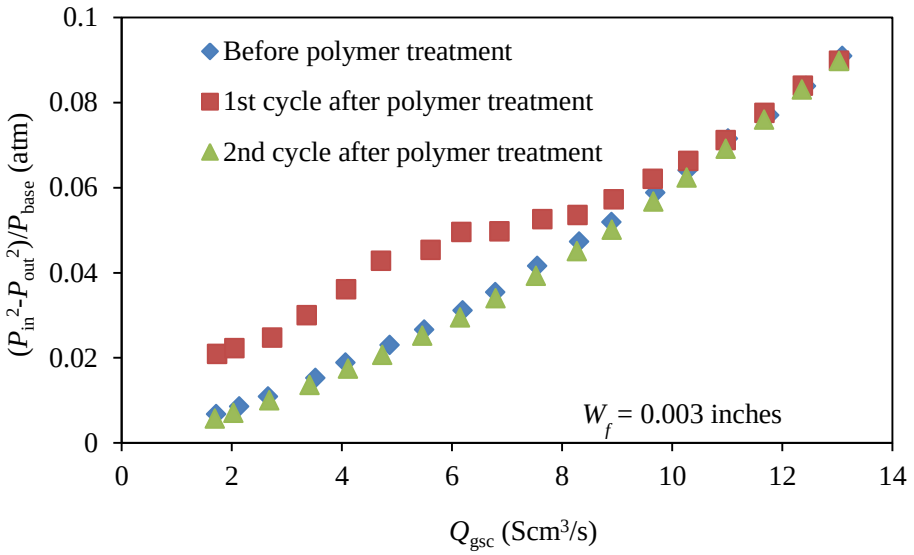

Figure 5.12. Comparison of $(P_{in}^2-P_{out}^2)/P_{base}$ before the Polymer Treatment and after the Polymer Treatment for Shale Fracture Model with a Fracture Width of 0.003 inches

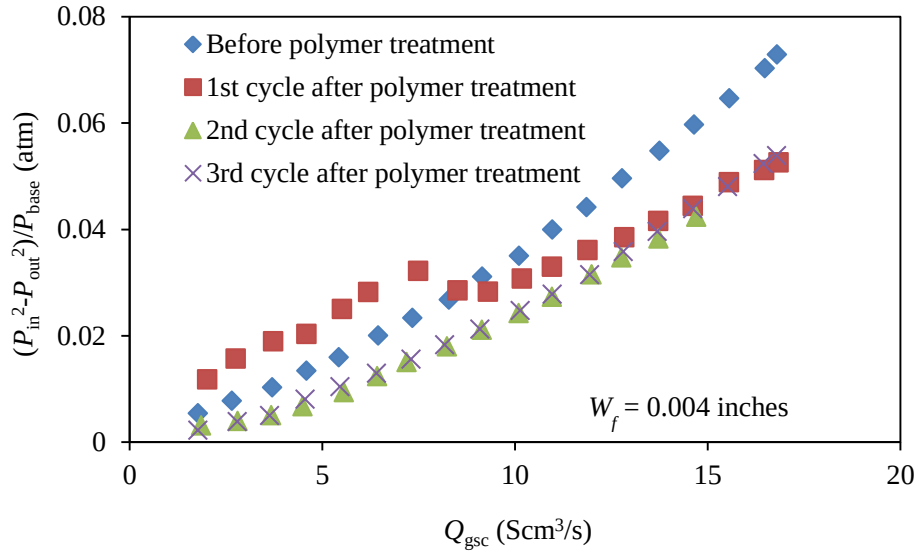

Figure 5.13. Comparison of $(P_{in}^2-P_{out}^2)/P_{base}$ before the Polymer Treatment and after the Polymer Treatment for Shale Fracture Model with a Fracture Width of 0.004 inches

The gas-injection pressure P_{in} and $(P_{in}^2-P_{out}^2)/P_{base}$ were smaller in the second and third cycles than in the first cycle. Furthermore, the data in the second and third cycles overlapped, indicating that the remaining polymer tended to stabilize within the fractures. As Figure 5.13 depicts, in the first cycle after the polymer treatment in

the widest fracture, the pressure response is higher than that before the polymer treatment for low flow rates, while it is smaller for high flow rates. The reason for this surprising result is the polymer was gradually flushed out during gas flooding from the lowest to the highest flow rates, and the resistance to gas flow was getting lower and lower. At the high flow rates, the polymer does not resist gas flow in the widest fracture, and may even improve it.

Based on the new approach for determining the $F_{rr,gas}$, the binomial equation $(P_{in}^2-P_{out}^2)/P_{base}$ as a function of the gas flow rate Q_{gsc} can be fitted well for each superficial gas velocity (i.e., $V_1 \sim V_6$) in Table 4.2. As detailed in Tables 5.5, 5.6 and 5.7, $(P_{in}^2-P_{out}^2)/P_{base}$ after the polymer treatment was calculated for each gas flow rate Q_{gsc} using fitting equations.

Table 5.5. $(P_{in}^2-P_{out}^2)/P_{base}$ after the Polymer Treatment for Shale Fracture Model with a Fracture Width of 0.002 inches

Superficial gas velocity (m/s)	Flow rate (Scm^3/s)	$(P_{in}^2-P_{out}^2)/P_{base}$ in the first cycle (atm)	$(P_{in}^2-P_{out}^2)/P_{base}$ in the second cycle (atm)	$(P_{in}^2-P_{out}^2)/P_{base}$ in the third cycle (atm)
$V_1 = 5$	$Q_1 = 1.372$	0.1784	0.0654	0.0654
$V_2 = 10$	$Q_2 = 2.743$	0.2656	0.1377	0.1385
$V_3 = 15$	$Q_3 = 4.115$	0.2995	0.2176	0.2187
$V_4 = 20$	$Q_4 = 5.486$	0.3569	0.3050	0.3056
$V_5 = 25$	$Q_5 = 6.858$	0.4176	0.4005	0.4000
$V_6 = 30$	$Q_6 = 8.230$	0.5055	0.5016	0.5006

Table 5.6. $(P_{in}^2-P_{out}^2)/P_{base}$ after the Polymer Treatment for Shale Fracture Model with a Fracture Width of 0.003 inches

Superficial gas velocity (m/s)	Flow rate (Scm^3/s)	$(P_{in}^2-P_{out}^2)/P_{base}$ in the first cycle (atm)	$(P_{in}^2-P_{out}^2)/P_{base}$ in the second cycle (atm)
$V_1 = 5$	$Q_1 = 2.057$	0.0223	0.0072
$V_2 = 10$	$Q_2 = 4.115$	0.0364	0.0174
$V_3 = 15$	$Q_3 = 6.172$	0.0496	0.0297
$V_4 = 20$	$Q_4 = 8.230$	0.0533	0.0447
$V_5 = 25$	$Q_5 = 10.287$	0.0662	0.0625
$V_6 = 30$	$Q_6 = 12.344$	0.0836	0.0828

Table 5.7. $(P_{in}^2-P_{out}^2)/P_{base}$ after the Polymer Treatment for Shale Fracture Model with a Fracture Width of 0.004 inches

Superficial gas velocity (m/s)	Flow rate (Scm^3/s)	$(P_{in}^2-P_{out}^2)/P_{base}$ in the first cycle (atm)	$(P_{in}^2-P_{out}^2)/P_{base}$ in the second cycle (atm)	$(P_{in}^2-P_{out}^2)/P_{base}$ in the third cycle (atm)
$V_1 = 5$	$Q_1 = 2.743$	0.0156	0.0039	0.0037
$V_2 = 10$	$Q_2 = 5.486$	0.0249	0.0092	0.0105
$V_3 = 15$	$Q_3 = 8.230$	0.0292	0.0179	0.0184
$V_4 = 20$	$Q_4 = 10.973$	0.0330	0.0274	0.0278
$V_5 = 25$	$Q_5 = 13.716$	0.0416	0.0382	0.0397
$V_6 = 30$	$Q_6 = 16.459$	0.0511	0.0508	0.0524

Eq. (4) was used to calculate the $F_{rr,gas}$ at different superficial gas velocities in different cycles after the polymer treatment. The relationship between $F_{rr,gas}$ and

superficial gas velocity V are plotted in Figures 5.14, 5.15 and 5.16 for the three shale fracture models, respectively. A similar result was found in gas-injection experiments on the three shale fracture models.

In the first cycle, the $F_{rr,gas}$ decreased as the superficial gas velocity increased. This phenomenon, which was similar to that observed for the $F_{rr,water}$, occurred because gas gradually flushed more and more polymer out of the shale fracture models. In addition, higher superficial gas velocity squeezed the polymer coating on the fracture surfaces more, creating larger channels through which gas can pass.

For the same shale fracture model, the $F_{rr,gas}$ in the second and third cycles was smaller than that in the first cycle at the same superficial gas velocity. The $F_{rr,gas}$ was almost the same in the second and third cycles, and did not change much with the superficial velocity. This indicates that the distribution of remaining polymer tended to stabilize in the fractures.

Besides, as shown in Figure 5.16, in the first cycle after the polymer treatment in the widest fracture, the $F_{rr,gas}$ is larger than one for low superficial gas velocities, while it is less than one for high superficial gas velocities. This phenomenon is in agreement with that observed in Figure 5.13.

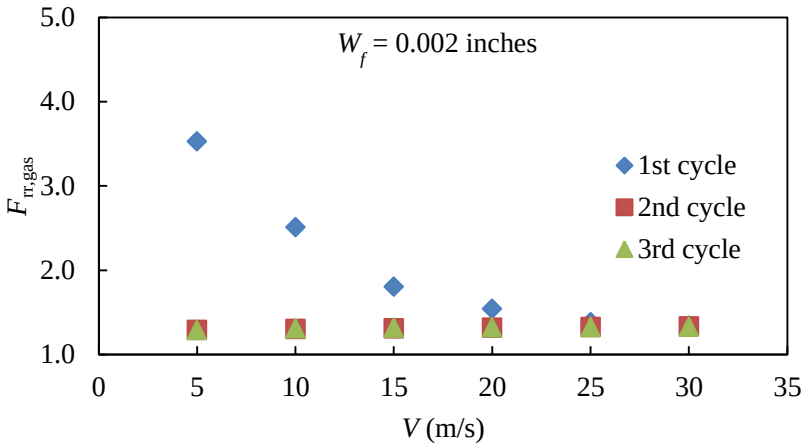

Figure 5.14. Relationship between $F_{rr,gas}$ and V for Shale Fracture Model with a Fracture Width of 0.002 inches

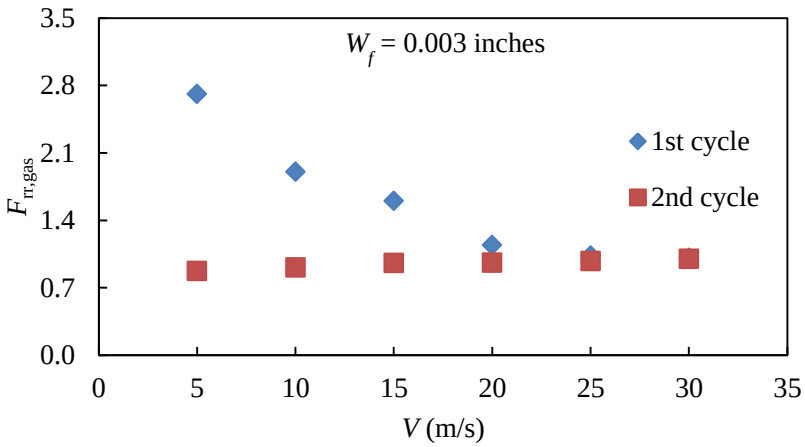

Figure 5.15. Relationship between $F_{rr,gas}$ and V for Shale Fracture Model with a Fracture Width of 0.003 inches

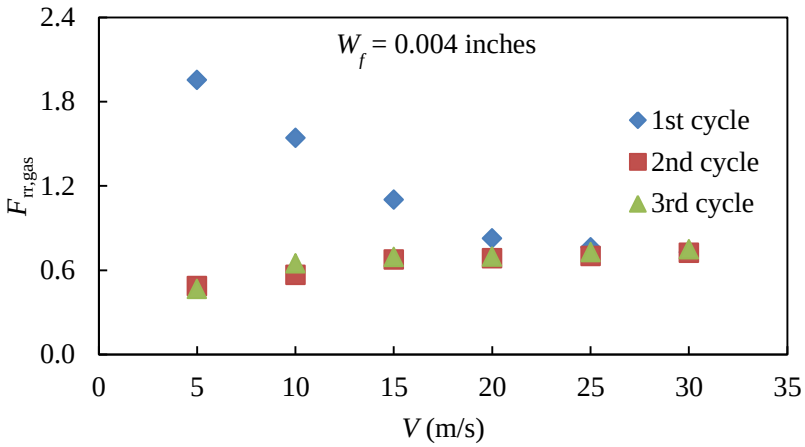

Figure 5.16. Relationship between $F_{rr,gas}$ and V for Shale Fracture Model with a Fracture Width of 0.004 inches

Figure 5.17 shows $F_{rr,gas}$ for all fracture widths as a function of superficial gas velocity on a log-log scale. In the first cycle, the relationship between the $F_{rr,gas}$ and the superficial gas velocity was fitted well by a power-law equation:

$$F_{rr,gas} = \beta V^{n} \tag{6}$$

Where β and n are coefficients related to the experimental conditions; and V is the superficial gas velocity, m/s.

Table 5.8 lists the coefficients of fitting equation and correlation factors for the three shale fracture models. The agreement was good for all of the equations.

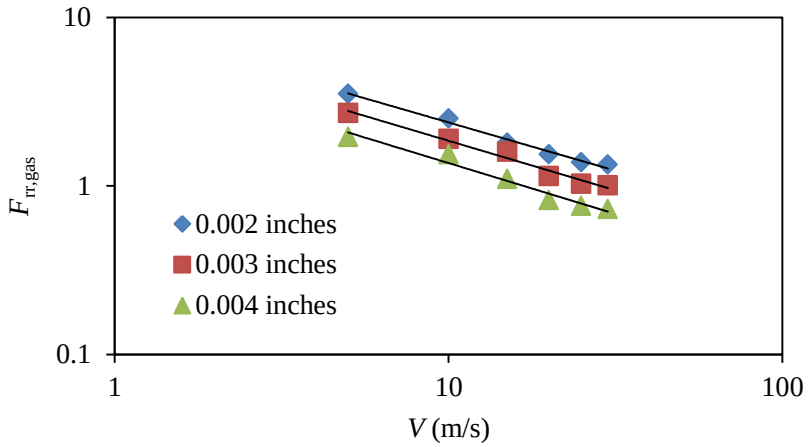

Figure 5.17. Comparison of $F_{rr,gas}$ at Different Fracture Widths in the First Cycle after the Polymer Treatment

Table 5.8. Coefficients of Fitting Equation for $F_{rr,gas}$ as a Function of Superficial Gas Velocity

Fracture width (inches)	Coefficient in fitting equation		R^2
	β	n	
0.002	8.886	-0.572	0.9866
0.003	7.175	-0.588	0.9754
0.004	5.487	-0.603	0.9654

As Figure 5.17 depicts, the narrower a fracture, at the same superficial gas velocity, the bigger the $F_{rr,gas}$. In the three shale fracture models, the $F_{rr,gas}$ was smaller than the $F_{rr,water}$. This phenomenon indicates that the polymer treatment selectively reduced the permeability to water more than to gas.

Another surprising finding is that the $F_{rr,gas}$ was less than one in the two shale fracture models with fracture widths of 0.003 inches and 0.004 inches when the $F_{rr,gas}$ tended to stabilize after the polymer treatment. This finding indicates that polymer treatment does not impair gas flow in wider fractures, and may even improve it. This could be attributed to the double effect that polymer treatment may have on gas flow

in shale fractures; it may reduce the fracture width, leading to a decrease in gas permeability, and also coat the shale surface, which could reduce the roughness of the rock surface, resulting in increased gas permeability.

6. CONCLUSIONS

This study evaluated the effect of polymer on water and gas flow behavior in fractured shale rocks. The major conclusions are summarized as follows:

- At lower water flow rates, the residual resistance factor for brine ($F_{rr,water}$) decreased as the shear rate increased, and the relationship was fitted well with a power-law equation. However, $F_{rr,water}$ tended to stabilize at high water flow rates. In addition, $F_{rr,water}$ was smaller in the wider fracture at the same shear rate.
- Brine flushed some polymer out in the first cycle after the polymer treatment. Therefore, the effect of polymer on water flow behavior weakened, and $F_{rr,water}$ was smaller in the second cycle after the polymer treatment.
- A new approach was developed to determine the residual resistance factor for gas ($F_{rr,gas}$) in order to evaluate the effect of polymer on gas flow behavior. In the first cycle after the polymer treatment, $F_{rr,gas}$ decreased as the superficial gas velocity increased, and the relationship was fitted well with a power-law equation. The wider fracture exhibited a smaller $F_{rr,gas}$ at the same superficial gas velocity.
- The $F_{rr,gas}$ was almost the same in the second and third cycles after the polymer treatment, and did not change much with the superficial gas velocity. This means that the distribution of the remaining polymer on the surface of the fractures tended to stabilize.
- For the shale fracture models with different fracture widths, the $F_{rr,water}$ was much larger than the $F_{rr,gas}$, which indicates that the polymer resisted water flow more than gas flow in the shale fracture models.

- The $F_{rr,gas}$ was less than one in the shale fracture models with fracture widths of 0.003 inches and 0.004 inches when $F_{rr,gas}$ tended to stabilize after the polymer treatment. This surprising finding indicates that polymer treatment does not impair gas flow in wider fractures, and may even improve it.

BIBLIOGRAPHY

[1] EIA. Annual energy outlook 2014. http://www.eia.gov/forecasts/aeo/; 2014.

[2] Vincent MC. The next opportunity to improve hydraulic-fracture stimulation. Journal of Petroleum Technology 2012; 64(3): 118-127.

[3] Dong Z, Holditch S, McVay D. Resource evaluation for shale gas reservoirs. SPE Economics & Management 2013; 5(1): 5-16.

[4] Bai B, Elgmati M, Zhang H, Wei M. Rock characterization of Fayetteville shale gas plays. Fuel 2013; 105: 645-652.

[5] Zuber MD, Lee WJ, Gatens JM. Effect of stimulation on the performance of Devonian shale gas wells. SPE Production Engineering 1987; 2(4): 250-256.

[6] Page JC, Miskimins JL. A comparison of hydraulic and propellant fracture propagation in a shale gas reservoir. Journal of Canadian Petroleum Technology 2009; 48(5): 26-30.

[7] Apaydin OG, Ozkan E, Raghavan R. Effect of discontinuous microfractures on ultratight matrix permeability of a dual-porosity medium. SPE Reservoir Evaluation & Engineering 2012; 15(4): 473-485.

[8] Guo T, Zhang S, Qu Z, Zhou T, Xiao Y, Gao J. Experimental study of hydraulic fracturing for shale by stimulated reservoir volume. Fuel 2014; 128: 373-380.

[9] Wang Y, Miskimins JL. Experimental investigations of hydraulic fracture growth complexity in slickwater fracturing treatments. In: Tight gas completions conference, Society of Petroleum Engineers, San Antonio, Texas; 2010.

[10] Fisher MK, Wright CA, Davidson BM, Steinsberger NP, Buckler WS, Goodwin A, Fielder EO. Integrating fracture mapping technologies to improve simulations in the Barnett shale. SPE Production & Facilities 2005; 20(2): 85-93.

[11] Dayan A, Stracener SM, Clark PE. Proppant transport in slickwater fracturing of shale gas formations. In: SPE annual technical conference and exhibition, Society of Petroleum Engineers, New Orleans, Louisiana; 2009.

[12] Palisch TT, Vincent M, Handren PJ. Slickwater fracturing: Food for thought. SPE Production & Operations 2010; 25(3): 327-344.

[13] Kostenuk NH, Browne DJ. Improved proppant transport system for slickwater shale fracturing. In: Canadian unconventional resources and international petroleum conference, Society of Petroleum Engineers, Calgary, Alberta; 2010.

[14] Robb ID, Welton TD, Bryant J, Carter ML. Friction reducer performance in water containing multivalent ions. US Patent 7846878, assigned to Halliburton Energy Services, Inc., Duncan, Oklahoma; 2010.

[15] Kot E, Saini R, Norman LR, Bismarck A. Novel drag-reducing agents for fracturing treatments based on polyacrylamide containing weak labile links in the polymer backbone. SPE Journal 2012; 17(3): 924-930.

[16] Zhou J, Baltazar M, Sun H, Qu Q. Water-based environmentally preferred friction reducer in ultrahigh-TDS produced water for slickwater fracturing in shale reservoirs. In: SPE/EAGE European unconventional resources conference and exhibition, Society of Petroleum Engineers, Vienna, Austria; 2014.

[17] Zhou J, Sun H, Stevens RF, Qu Q, Bai B. Bridging the gap between laboratory characterization and field applications of friction reducers. In: SPE production and operations symposium, Society of Petroleum Engineers, Oklahoma City, Oklahoma; 2001.

[18] Sun Y, Wu Q, Wei M, Bai B, Ma Y. Experimental study of friction reducer flows in microfracture. Fuel 2014; 131: 28-35.

[19] Lescarboura JA, Culter JD, Wahl HA. Drag reduction with a polymeric additive in crude oil pipelines. Society of Petroleum Engineers Journal 1971; 11(3): 229-235.

[20] White CM, Mungal MG. Mechanics and prediction of turbulent drag reduction with polymer additives. Annual Review of Fluid Mechanics 2008; 40: 235-256.

[21] Sun H, Stevens RF, Cutler JL, Wood B, Wheeler RS, Qu Q. A novel nondamaging friction reducer: Development and successful slickwater frac applications. In: SPE eastern regional meeting, Society of Petroleum Engineers, Morgantown, West Virginia; 2010.

[22] Edomwonyi-Otu LC, Chinaud M, Angeli P. Drag reduction in stratified oil-water flows. In: 9th North American conference on multiphase technology, BHR Group, Banff, Canada; 2014.

[23] Carman PS, Cawiezel KE. Successful breaker optimization for polyacrylamide friction reducers used in slickwater fracturing. In: SPE hydraulic fracturing technology conference, Society of Petroleum Engineers, College Station, Texas; 2007.

[24] Kaufman PB, Penny GS, Paktinat J. Critical evaluation of additives used in shale slickwater fracs. In: SPE shale gas production conference, Society of Petroleum Engineers, Fort Worth, Texas; 2008.

[25] Montgomery C. Fracturing fluid components. In: ISRM international conference for effective and sustainable hydraulic fracturing, International Society for Rock Mechanics, Brisbane, Australia; 2013.

[26] Rivard C, Lavoie D, Lefebvre R, Séjourné S, Lamontagne C, Duchesne M. An overview of Canadian shale gas production and environmental concerns. International Journal of Coal Geology 2014; 126: 64-76.

[27] Seright RS. Reduction of gas and water permeabilities using gels. SPE Production & Facilities 1995; 10(2): 103-108.

[28] Al-Sharji HH, Grattoni CA, Dawe RA, Zimmerman RW. Disproportionate permeability reduction due to polymer adsorption entanglement. In: SPE European formation damage conference, Society of Petroleum Engineers, The Hague, Netherlands; 2001.

[29] Bai B, Liu Y, Coste JP, Li L. Preformed particle gel for conformance control: Transport mechanism through porous media. SPE Reservoir Evaluation & Engineering 2007; 10(2): 176-184.

[30] Bai B, Li L, Liu Y, Liu H, Wang Z, You C. Preformed particle gel for conformance control: Factors affecting its properties and applications. SPE Reservoir Evaluation & Engineering 2007; 10(4): 415-422.

[31] Zaitoun A, Kohler N. Two-phase flow through porous media: effect of an adsorbed polymer layer. In: SPE annual technical conference and exhibition. Houston, Texas: Society of Petroleum Engineers; 1988.

[32] Barreau P, Lasseux D, Bertin H, Glenat Ph, Zaitoun A. Polymer adsorption effect on relative permeability and capillary pressure: Investigation of a pore scale scenario. In: International symposium on oilfield chemistry. Houston, Texas: Society of Petroleum Engineers; 1997.

[33] Barreau P, Bertin H, Lasseux D, Glenat Ph, Zaitoun A. Water control in producing wells: influence of an adsorbed-polymer layer on relative permeabilities and capillary pressure. SPE Reser Eng 1997;12(4):234–9.

[34] Zaitoun A, Bertin H, Lasseux D. Two-phase flow property modifications by polymer adsorption. In: SPE/DOE improved oil recovery symposium. Tulsa, Oklahoma: Society of Petroleum Engineers; 1998.

[35] Zitha PLJ, Darwish MMI. Effect of bridging adsorption on the placement of gels for water control. In: SPE Asia pacific improved oil recovery conference. Kuala Lumpur, Malaysia: Society of Petroleum Engineers; 1999.

[36] Elmkies Ph, Bertin H, Lasseux D, Murray M, Zaitoun A. Further investigations on two-phase flow property modification by polymers: Wettability effects. In: SPE international symposium on oilfield chemistry. Houston, Texas: Society of Petroleum Engineers; 2001.

[37] Elmkies Ph, Lasseux D, Bertin H, Pichery T, Zaitoun A. Polymer effect on gas/water flow in porous media. In: SPE/DOE improved oil recovery symposium. Tulsa, Oklahoma: Society of Petroleum Engineers; 2002.

[38] Grattoni CA, Luckham PF, Jing XD, Norman L, Zimmerman RW. Polymers as relative permeability modifiers: adsorption and the dynamic formation of thick polyacrylamide layers. J Petrol Sci Eng 2004;45(3–4):233–45.

[39] Blanchard V, Lasseux D, Bertin H, Pichery T, Chauveteau G, Tabary R, et al. Gas/water flow in porous media in the presence of adsorbedpolymer:experimental study on non-Darcy effects. SPE Reservoir Eval En2007;10(4):423–31.

[40] Paktinat, J., O'Neil, B. J. and Tulissi, M. G. 2011. Case Studies: Impact of High Salt Tolerant Friction Reducers on Freshwater Conversation in Canadian Shale Fracturing Treatments. Presented at the Canadian Unconventional Resources Conference, Alberta, Canada, 15-17 November 2011. SPE-149272-MS.

[41] White, G. L. 1964. Friction Pressure Reducers in Well Stimulation. Journal of Petroleum Technology 16 (8): 865 - 86810.2118/802-PA.

[42] Liang, J.-T., Sun, H., & Seright, R. S. (1995, November 1). Why Do Gels Reduce Water Permeability More Than Oil Permeability? Society of Petroleum Engineers. doi:10.2118/27829-PA

[43] Imqam, A. H., Bai, B., Xiong, C., Wei, M., Delshad, M., & Sepehrnoori, K. (2014, October 14). Characterisations of Disproportionate Permeability Reduction of Particle Gels Through Fractures. Society of Petroleum Engineers. doi:10.2118/171531-MS

[44] Liang, J., & Seright, R. S. (2000, January 1). Wall-Effect/Gel-Droplet Model of Disproportionate Permeability Reduction. Society of Petroleum Engineers. doi:10.2118/59344-MS

[45] Liang, J., & Seright, R. S. (2001, September 1). Wall-Effect/Gel-Droplet Model of Disproportionate Permeability Reduction. Society of Petroleum Engineers. doi:10.2118/74137-PA

[46] Zaitoun, A., Bertin, H., & Lasseux, D. (1998, January 1). Two-Phase Flow Property Modifications by Polymer Adsorption. Society of Petroleum Engineers. doi:10.2118/39631-MS

[47] Willhite, G. P., Zhu, H., Natarajan, D., McCool, C. S., & Green, D. W. (2002, March 1). Mechanisms Causing Disproportionate Permeability Reduction in Porous Media Treated With Chromium Acetate/HPAM Gels. Society of Petroleum Engineers. doi:10.2118/77185-PA

[48] Ganguly, S., Willhite, G. P., Green, D. W., & McCool, C. S. (2003, January 1). Effect of Flow Rate on Disproportionate Permeability Reduction. Society of Petroleum Engineers. doi:10.2118/80205-MS

[49] Seright, R. S. (2006, January 1). Optimizing Disproportionate Permeability Reduction. Society of Petroleum Engineers. doi:10.2118/99443-MS

[50] Liang, J.-T., & Seright, R. S. (1997, November 1). Further Investigations of Why Gels Reduce Water Permeability More Than Oil Permeability. Society of Petroleum Engineers. doi:10.2118/37249-PA

[51] Al-Sharji, H. H., Grattoni, C. A., Dawe, R. A., & Zimmerman, R. W. (1999, January 1). Pore-Scale Study of the Flow of Oil and Water through Polymer Gels. Society of Petroleum Engineers. doi:10.2118/56738-MS

[52] Ogunberu, A. L., & Asghari, K. (2004, January 1). Water Permeability Reduction Under Flow-Induced Polymer Adsorption. Society of Petroleum Engineers. doi:10.2118/89855-MS

[53] Elmkies, P., Bertin, H., Lasseux, D., Murray, M., & Zaitoun, A. (2001, January 1). Further Investigations on Two-Phase Flow Property Modification by Polymers: Wettability Effects. Society of Petroleum Engineers. doi:10.2118/64986-MS

VITA

In May, 2014, Lingbo Liu received his dual Bachelor of Science degrees in Petroleum Engineering from Missouri University of Science and Technology and China University of Petroleum in Beijing. He received his Master of Science degree in Petroleum Engineering from Missouri University of Science and Technology in May, 2015.